DCE 19 3rd DOCTORAL CONGRESS IN ENGINEERING

DOCTORAL CONGRESS in ENGINEERING

Book of Abstracts

Symposium on Engineering Physics

U.PORTO
FEUP FACULDADE DE ENGENHARIA
UNIVERSIDADE DO PORTO

DCE 19 3rd DOCTORAL CONGRESS IN ENGINEERING

Book of Abstracts

of the

Symposium on Engineering Physics

Editors:
A. Silva, J. Villate, J. Oliveira, M. Braga

Porto
June 2019

This volume contains the abstracts presented at the Symposium on Engineering Physics, within the 3rd Doctoral Congress in Engineering - DCE19, held in FEUP, Porto, between June 27th and 28th, 2019.

Title: Book of Abstracts of the Symposium on Engineering Physics

Edited by A. Silva, J. Villate, J. Oliveira, M. Braga

Published by: FEUP Edições

https://sigarra.up.pt/feup/pt/pub_geral.pub_view?pi_pub_base_id=331608

First edition, June 2019

ISBN. 978-972-752-250-7

Universidade do Porto, Faculdade de Engenharia, Departamento de Engenharia Física, Rua Dr. Roberto Frias s/n 4200-465 Porto, Portugal

WELCOME

Modern engineering increasingly faces the challenges of including state of the art physics knowledge and research results. Engineering Physics aims to bridge these inter- and multi-disciplinary physics developments with the diverse engineering fields. It plays a crucial role in the creation of novel technological solutions with potentially high impact in society.

The Doctoral Symposium on Engineering Physics of 2019 took place from June 27 to 28, 2019, in the Doctoral Congress in Engineering at the Faculty of Engineering of the University of Porto. It was organized jointly by the Department of Physics Engineering of the School of Engineering and the Physics and Astronomy Department of the School of Sciences. The third of such events, it received contributions from all the major Portuguese research institutions active in this field at a doctoral level, including the leading universities in Portugal. This book presents extended abstracts of the communications delivered during the symposium. These communications offered a clear glimpse of the current trends in this area in Portugal and covered topics as varied as new materials, nanodevices, instruments, optoelectronics, and biomedical devices.

The meeting gathered young and senior Engineering Physics researchers. It included two inspiring keynote lectures by Prof. Vitor Amaral from the University of Aveiro and by Prof. Helena Braga from the University of Porto, both leading researchers in their fields.

It is a pleasure to acknowledge all the participants for the productive and pleasant atmosphere of the Symposium. Special acknowledgments are due to the Doctoral Congress supporters, and the Congress Scientific and Organizing Committees.

Porto, June 2019

Symposium Organizing Committee

CONTENTS

CONTENTS

COMMITTEES

Symposium Scientific Committee

Chair: Joana Espain | FEUP

Adriano Carvalho | FEUP
André Pereira | FCUP
António Cunha | U. Aveiro
Bernardo Almeida | U. Minho
Carla Rosa | FCUP
Hélder Crespo | FCUP
Helena Braga | FEUP
Henrique Salgado | FEUP
Inês Carvalho | FEUP
Jaime Villate | FEUP
Joana Oliveira | FEUP
João Pedro Araújo | FCUP
João Ventura | FCUP
José Rebordão | FCUL
Isabel Catarino | NOVA
Isabel Lopes | FCUC
Luísa Andrade | FEUP
Manuel Alves | FEUP
Manuel Vieira | FEUP
Maria de Jesus | NOVA
Mário Pimenta | IST
Olinda Conde | FCUL
Paulo Marques | FCUP
Paulo Sá | FEUP
Pedro Alpuim | U. Minho
Pedro Camanho | FEUP
Pedro Jorge | FCUP
Susana Freitas | IST
Vítor Amaral | U. Aveiro

PROGRAMME

Symposium chair: **Joana Espain**
Location: **B030**

Session 1 | 27th June, 10h30 - 13h00 (Chair: João Pedro Araújo)

Symposium Keynote Lecture, Vítor Amaral

- Carbon-based Materials for Thermoelectric Conversion, Ana Sousa
- Thermoelectric Materials for new innovative devices: from nanoparticles to composites, Margarida Maia
- Magnetic dipolar synchronization of vortex-based spin torque nano oscillators with independent top contacts, Leandro Martins
- Local probe studies on the naturally layered Ca2MnO4, Pedro Rocha
- Local Probing on Ferrolelectric $Ca_{n+1}Ti_nO_{3n+1}$ naturally layered perovskite, Tiago Leal

Session 2 | 27th June, 14h30 -17h00 (Chair: Joana Espain)

Symposium Keynote Lecture, Helena Braga

- A multi-grating triboelectric nanogenerator for maritime applications, Cátia Rodrigues
- Wearable Textile Supercapacitor based on Nitrogen-doped Carbon Nanomaterial, Rui Costa
- Solid-state batteries with ferroelectric electrolyte and polymer composites, Rita Veloso
- Optical analogues of superfluids in Nematic Liquid Crystals, Tiago Ferreira
- Non-Destructive Testing Using Advanced Magnetorheological Elastomers, Joana Silva

Session 3 | 28th June, 9h00 -10h30 (Chair: Paulo Marques)

- Fabry-Pérot interferometer fabricated in fused silica through femtosecond laser micromachining, João Maia
- Low-loss broadband femtosecond laser written surface waveguides for enhanced evanescent coupling, Vítor Amorim
- Fabrication of periodic structures in optical fibers by femtosecond laser micromachining, Duarte Viveiros
- Laser induced breakdown system optimization and its applications, Miguel Ferreira

Poster session (with general congress) | 28th June, - 10h30-11h30

- Sofia Ferreira-Teixeira, Ana L. Pires, Will R. Branford, João P. Araújo, Lesley F. Cohen and André M. Pereira. The Topological Surface State on a Variable Range Hopping dominated conduction Sb2Te3 sputtered thin film
- Paula Quitério, Arlete Apolinário, Célia Sousa, Paula Dias, João Azevedo, Adélio Mendes and João Araujo. 1D Hematite photoanodes for photoelectrochemical hydrogen production
- Sandra Rodrigues, Joana Paiva, Paulo Marques, João Cunha and Pedro Jorge. Trapping nanometer sized particles with optical fiber tweezers – a computational study
- João Magalhães, André Pereira, Ana Pires and Clara Pereira. On the Development of Organic and Inorganic Thermoelectric Materials for Printing Techniques
- Paulo Robalinho and Orlando Frazão. Fiber micro-cantilever displacement detection
- Filipe Marques and Orlando Frazão. Transmission Properties of Optical Fibers during Taper Fabrication: Adiabaticity, Mode Dissipation, and Diameter Control
- Tiago D. Ferreira, Nuno A. Silva, O. Bertolami, C. Gomes and Ariel Guerreiro. Exploring cosmological systems under alternative theories of gravity using the Schrödinger-Poisson formalism
- Tiago D. Ferreira, Nuno A. Silva and Ariel Guerreiro A multidimensional solver of the generalized Schrödinger equation based on GPGPU supercomputing
- Rui Fernandez, Guiomar Evans, José Augusto, Luis Gurriana and Agostinho Gomes Low Noise Power Supply Board
- Filipe Cuim, José Augusto, Guiomar Evans, Agostinho Gomes and Filipe Martins. Functional Tester for High Voltage Boards of the TileCal Calorimeter
- João Mendes, Luís Coelho, Carlos Pereira, Barna Kovács, Pedro Jorge and Teresa Borges. New Optochemical sensor for dissolved CO2 evaluation: results from application to a recirculation aquaculture system and bacterial microcosms
- Helena Vasconcelos, Almeida, Saraiva, Jorge and Coelho. Detection of hydrogen peroxide using a chemiluminescence technique: preliminary study
- José Brandão, Joana Oliveira and Maria Braga. Effect of radiation on the electrolyte of a solid-state battery
- João M. Serra, Sara Sequeira, Ismael Domingos, Ana Oliveira, Ermelinda Maçôas, Susana Cardoso, Helena Alves and Diana Leitão. Micropatterning Organic Single Crystals for Photonic Sensor Applications

Session 3 | 28th June, 11h30 -13h00 (Chair: Paulo Marques)

- Optical properties of a composite layer containing graphene and plasmonic particles, Tiago Queirós
- Vibration detection on power transformers using optical fiber sensors, Catarina Monteiro
- Fibre-integrated phase-change devices, Tiago Martins
- Fabrication of RFID antennas in thin membranes of Parylene-C for wearable applications, Leonor Duarte

Session 4 | 28th June, 14h00 - 15h30 (Chair: André Pereira)

- Graphene Radio-Frequency Transistors with Self-Aligned Channel and Core-Shell Nanowire Gate, Lucas Baptista
- Development of a Dual-Polarity Ion Drift Chamber, David Marques
- A One-Pot Synthesis Method of Chitosan Magnetic Composite Structures for Sensing in Biomedicine, Francisca Gomes
- Image Processing and Object Detection for ADAS, André Gabriel

KEYNOTE SPEAKERS

Vitor Amaral

Physics Department, University of Aveiro/ CICECO, Aveiro Institut for Materials

Topic: Quantum sensing technologies

Vitor Amaral was born in 1962 and obtained his PhD in Condensed Matter Physics at the University of Porto in 1993 and is presently Professor Catedrático (since 2009) at the Physics Department of the University of Aveiro.

His main research interests are related to magnetism and multiferroic phenomena in complex oxides, thin films and nanoparticles and on the application of nuclear solid state techniques. Recent topics are magnetothermal, and magnetostructural effects and their applications in refrigeration and thermal management processes.

He is a researcher at Laboratório Associado CICECO-Aveiro Institute of Materials and Coordinator of Group 2. “Multifunctional Ferroic Ceramics and Nanostructures” and also at ISOLDE-CERN (Switzerland), where he is spokesperson of projects on the application of radioactive isotopes for hyperfine studies on graphene, magnetic nanoparticles and multiferroic materials.

He was Vice-President of the Portuguese Physical Society (2004-2007) and Coordinator of EMMS (Joint European Master on Materials Science) of the Erasmus Mundus Programme (2007-2013), a consortium of the Universities of Aveiro, Aalborg and Technical University of Hamburg-Harburg.

He is author/co-author of more than 240 scientific publications in SCI index and 1 patent. Principal Researcher of over 10 Projects funded by Fundação para a Ciência e Tecnologia, and 5 projects at CERN-ISOLDE. Coordinator of 6 bi-lateral collaboration projects (Brasil, India, Germany, Italy and 2 with Spain).

Maria Helena Braga

Department of Engineering Physics, Faculty of Engineering, University of Porto / LAETA

Topic: Back to 1D: Rethinking all-solid-state energy storage architectures with a ferroelectric-electrolyte

Maria Helena Braga is a Solid-State Physicist who has a PhD in Materials Science and Engineering. She is an Associate Professor and the Head of the Department of Engineering Physics at FEUP-UPORTO.

From 2008-2011 she has worked in the Los Alamos Neutron Scattering Center, USA, as a Research Scholar and Long Term Visiting Staff Member and during 2016-2019 she worked as Senior Research Fellow at the University of Texas at Austin where she brought lithium and sodium ferroelectric glass-electrolytes and new architecture devices developed in Portugal and collaborated with Prof. John Goodenough, Nobel of Chemistry 2019, in further developing these and other energy harvesting and storage devices.

AWARDS

Symposium on Engineering Physics

Best oral communication Award

Margarida Maia

Thermoelectric Materials for new innovative devices: from nanoparticles to composites

Best poster presentation Award (in ex aequo)

João M. Serra, Sara Sequeira, Ismael Domingos, Ana Oliveira, Ermelinda Maçôas, Susana Cardoso, Helena Alves and Diana Leitão.

Micropatterning Organic Single Crystals for Photonic Sensor Applications.

and

Sandra Rodrigues, Joana Paiva, Paulo Marques, João Cunha and Pedro Jorge.

Trapping nanometer sized particles with optical fiber tweezers – a computational study.

ORAL PRESENTATIONS

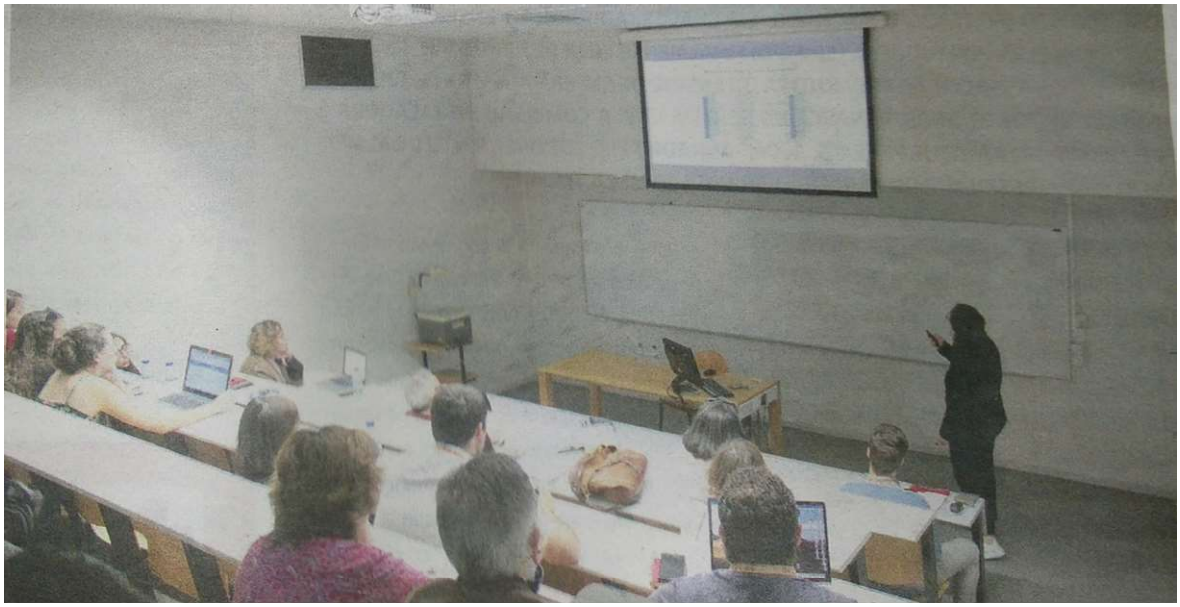

Carbon-based Materials for Thermoelectric Conversion

Ana R. C. Sousa[1,2], O. Salomé, G.P. Soares[2], Ana L. Pires[1], Clara Pereira[3], Manuel F. R. Pereira[2], André M. Pereira[1]

[1]IFIMUP and IN- Institute of Nanoscience and Nanotechnology, Physics and Astronomy Department, University of Porto, Rua do Campo Alegre s/n, 4169-007 Porto, Portugal
[2]Laboratory of Catalysis and Materials (LCM), Associate Laboratory LSRE/LCM, Department of Chemical Engineering, Faculty of Engineering, University of Porto, 4200-465 Porto, Portugal
[3]REQUIMTE/LAQV, Chemistry and Biochemistry Department, Faculty of Sciences, University of Porto, Rua do Campo Alegre s/n, 4169-007 Porto, Portugal.

Abstract

Thermoelectric Generators have a wide range of applications and can be an important way of turning the world into a more sustainable place through the recovery of wasted heat. Carbon-based materials bring a new opportunity in the thermoelectric field due to their abundant source, cheapness, non-toxicity and flexibility. The transport properties of these materials can be improved through chemical, mechanical and thermal treatments. The focus of the present work is to tune the thermoelectric properties of multi-walled carbon nanotubes (MWCNTs) and graphene nanoplatelets (GN) by using different functionalizations process such as HNO_3, melamine, ball milling and thermal treatments in N_2 atmosphere. Morphological, structural and textural analyses are discussed to understand the changes observed in the thermoelectric properties of the functionalized materials.

Author Keywords. MWCNT, Graphene, Thermoelectric properties, doping, nanocomposites

1. Introduction

Thermoelectric (TE) effect refers to the direct conversion of a heat flow into generation of an electromotive force and vice-versa. The performance of the TE materials can be quantified by their specific dimensionless figure of merit (zT) that depends on the electrical conductivity (σ), Seebeck Coefficient (S) and thermal conductivity (κ).

Inorganic materials are dominantly used in the field of TE materials mainly composed by semiconductors, intermetallics and even oxides. Carbon-based TE materials are also studied because they offer complementary advantages when compared with the other inorganic materials such as abundant source, low cost, non-toxicity, high temperature stability and light-weight[1]. Low dimensioned allotropes of carbon such as graphene and Carbon Nanotubes (CNTs) offer an opportunity in exploiting this particularity to enhance the density of states due to quantum confinement effects as a way of increasing the zT. Carbon materials have both porosity and high surface area that allows accessibility in the surface for the absorption of redox molecules[2]. This way, these materials could be doped with charge transfer dopants as a way of tuning the carrier density and the Fermi level leading to an alteration of the σ, the *S*. Due to the nanometer size in the diameter, it is also possible to affect the phonon mean free path, modifying the lattice contribution of the *k*.

2. Materials and Methods

In this work, Multiwalled Carbon Nanotubes (MWCNTs) and Graphene Nanoplatelets were subjects of different treatments – chemical (nitric acid and melamine), mechanical (ball milling) and thermic (furnace at different temperatures) – figure 1. The samples that arise from these treatments were studied in their bulk form through pressed powders.

A calculation of the power factor (PF) and figure of merit (zT) were carried out as ways of quantify the TE performance. Homemade setups were used to measure the Seebeck coefficient and thermal conductivity, and a 4 contact method was used to measure R and calculate the σ for the different types of the functionalized materials. Different characterization techniques were used as a way of analysing the changes performed in the different samples - structural characterizations, thermal desorption spectroscopy (TPD), thermogravimetric analysis (TGA), point of zero charge PH (PHpzc) and X-ray diffraction (XRD). The textural characterization of the materials, namely the Brunauer-Emmett-Teller (BET) surface area was based on the N2 adsorption isotherm. The pore size distribution was obtained by using the non-local density functional theory (NLDFT) applying the kernel file where a cylindrical-pore is assumed.

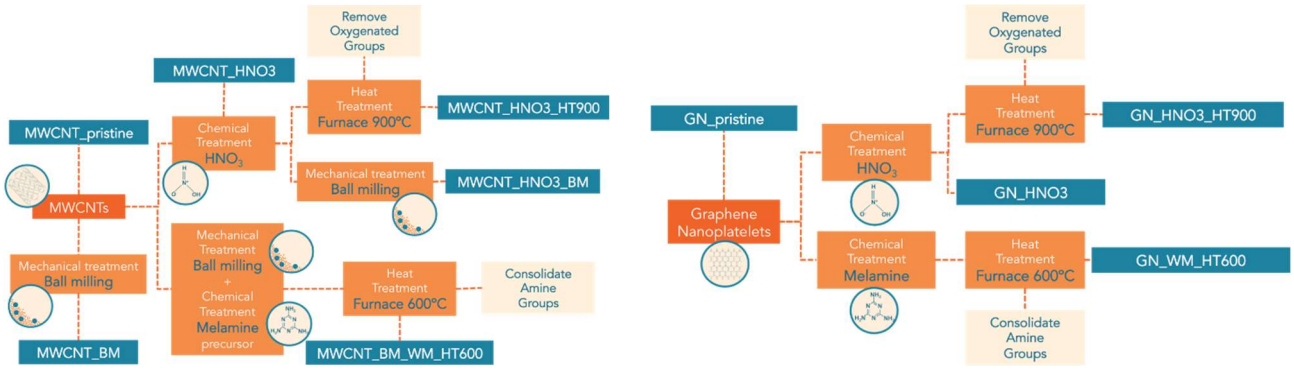

Figure 1: Schematic of the treatments used to obtain the functionalized MWCNTs samples (left) and GN samples (right) and respective used nomenclature

3. Discussion & Conclusions

It was found that MWCNT is a promising carbon material for improving the TE performance since it was verified an improvement of the main parameters of the zT in all functionalized materials (relative to the pristine sample). In contrast, graphene showed deterioration in almost of these parameters when performed similar treatments. Through the characterization techniques, it was possible to verify that the functionalizations dramatically altered the materials provoking changes in the carrier density, band structure, morphology, structure and in the scattering phenomena.

It was possible to achieve an improvement of two orders of magnitude in the zT for MWCNTs being the best-functionalized sample a result of an acid nitric and ball-milling combo. Nitric acid treatment and ball milling revealed as good techniques to functionalize MWCNTs with the aim of improving their TE performance.

References

[1] P. Chakraborty, T. Ma, A. H. Zahiri, L. Cao, and Y. Wang, “Carbon-Based Materials for Thermoelectrics,” *Adv. Condens. Matter Phys.*, vol. 2018, no. 3, pp. 1–29, 2018.

[2] J. L. Blackburn, A. J. Ferguson, C. Cho, and J. C. Grunlan, “Carbon-Nanotube-Based Thermoelectric Materials and Devices,” *Adv. Mater.*, vol. 30, no. 11, pp. 1–35, 2018.

Thermoelectric Materials for new innovative devices: from nanoparticles to composites

Margarida Maia[1], Ana L. Pires[1], Armandina M. L. Lopes[1], André M. Pereira[1]

[1]IFIMUP-IN – Material Physics Institute of University of Porto, Departamento de Física e Astronomia da Faculdade de Ciências da Universidade do Porto, Rua Campo Alegre, 687, 4769-007 Porto, Portugal.

Abstract

Thermoelectric (TE) Generators allow the transformation of thermal into electric energy, emerging as one of the highest impact mechanism of energy harvesting. The efficiency of a TE material can be measured by its Figure of Merit (**ZT**), which depends on the Seebeck Coefficient (**S**), the Electrical (**σ**) and Thermal Conductivities **(k**). One of the most promising strategies for their improvement consists of tailoring **k** using nanostructuring via phonon scattering. For this purpose, the chosen materials for this work were Bi2Te3, which is seen as a prime thermoelectric material with high efficiency at room temperature, and ZnO, due to its characteristics as an oxide TE material, e.g. its easy and cheap fabrication. In the first part of this work, there were fabricated and characterized ZnO nanoparticles, where it was possible the manipulation of their morphology which significantly affected the transport properties, namely at the lattice level, influencing the movement of the phonons. In the second part, there were incorporated the ZnO nanoparticles into a Bi_2Te_3 matrix to study another method of nanomanipulation.

Author Keywords. Thermoelectric, Zinc Oxide, Nanoparticles, Bismuth Telluride, Energy harvesting, Phonon scattering.

1. Introduction

Humanity is constantly growing and changing at an astounding pace, and with that comes great technological development, in which energy harvesting plays a fundamental role in our world sustainability. Since we live in an Internet of Things (IoT) era, alternative ways to produce energy, especially without the need to change batteries, have been strongly researched. Due to their simplicity, and possible flexibility and low-cost, thermoelectric materials and devices has been highly researched due to their high technological potential.

The thermoelectric effect is defined as the direct conversion of a temperature gradient into a voltage. This effect depends directly on the Seebeck Coefficient of the material, which directly relates the generated voltage with the applied gradient ($\Delta T=S\ \Delta V$), and the electrical conductivity, and inversely on the thermal conductivity.

Regarding these three parameters, the **S** and the **σ** depend on the band structure, i.e. the movement of the electrons. On the other hand, the **k** has two different components, the electronic one that also depends on the band structure, and the phononic one, that depends on the crystallographic lattice of the material. For this reason, the best strategy to increase the effect is by only manipulating the phononic component of the *k*, whilst the other parameters remain constant.

2. Discussion

Firstly, there were fabricated ZnO nanoparticles by a chemical co-precipitation route based on the addition of two solutions: zinc salt and the sodium hydroxide. It was possible to manipulate the preferential direction and the morphology of ZnO (passing from hexagonal prism-shaped particles to 'desert-rose stones'), by only varying the concentration of the NaOH in the co-precipitation Figure . During the morphologic change, the phononic

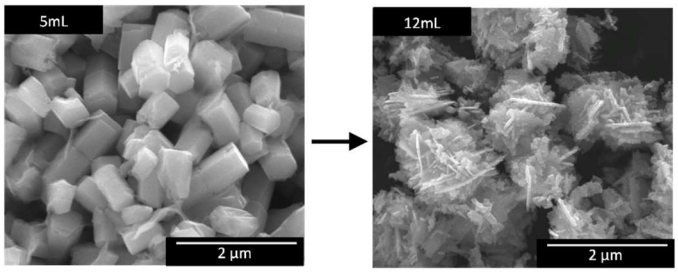

Figure 1 Morphology changes of the Zinc Oxide nanoparticles, due to the increase of the volume of NaOH in the co-precipitation process. The structures change from a hexagonal prism shape to “desert-rose stones”.

phenomena predominate on the **k**, where the structures are smaller (~50nm), compared with the clusters formed afterwards (~4µm). It was also possible to reduce the thermal conductivity by 30% (0.9 $Wm^{-1}K^{-1}$) due to the occurrence of quantum confinement.

Secondly, there were produced thermoelectric composites of microparticles of Bi_2Te_3 and nanoparticles of ZnO. The inclusion of nanoparticles in the Bi2Te3 matrix caused a ”coating” of the Bi_2Te_3 particles by the ZnO structures, compressing them, causing an increase in the microstrain of the Bi_2Te_3 lattice. Being a composite, a percolation model for the electrical conductivity is considered. The results show that the composites structure was of great complexity and full of irregular interfaces. Regarding the values of the thermal conductivity, it presents small variations around 1 W $m^{-1}K^{-1}$, only having the phononic influence.

References

T. M. Tritt and M. A. Subramanian, “Thermoelectric Materials, Phenomena, and Applications: A Bird’s Eye View”, MRS Bulletin, vol. 31, no. 3, pp. 188-198, 2006.

J.P. Heremans, M.S. Dresselhaus, L.E. Bell and D.T. Morelli, “When thermoelectrics reached the nanoscale”, Nature Nanotechnology, vol. 8, no. 7, pp. 471-473, 2013.

Y. Mamunya, V. Davydenko, P. Pissis, and E. Lebedev, “Electrical and thermal conductivity of polymers filled with metal powders,” European Polymer Journal, vol. 38, no. 9, pp. 1887–1897, 2002.

J. Li, Q. Tan, J.-F. Li, D.-W. Liu, F. Li, Z.-Y. Li, M. Zou, and K. Wang, “BiSbTe-based nanocomposites with high ZT : The effect of SiC nanodispersion on thermoelectric properties,” Advanced Functional Materials, vol. 23, no. 35, pp. 4317–4323, 2013.

Acknowledgements

The authors acknowledge Fundação para a Ciência e Tecnologia for financial support through the projects: PTDC/CTM-MAN/5414/2014.

Magnetic dipolar synchronization of vortex-based spin torque nano-oscillators with independent top contacts

Leandro Martins[1], Alex Jenkins[2], João Ventura[1] and Ricardo Ferreira[2]

1 IFIMUP-IN, Rua do Campo Alegre, 678, 4169-007 Porto, Portugal
2 INL, Avenida Mestre José Veiga, s/n, 4715-330 Braga, Portugal

Abstract
This work shows the first results of an ongoing study, regarding the synchronization of vortex-based spin torque nano-oscillators (STNOs). STNOs are novel nanoscopic microwave oscillators based on spintronic magnetic tunnel junctions (MTJs). Here, one aims to surpass the major roadblock still preventing the wide spread application of STNOs by integrating and synchronizing an array of STNOs to increase the delivered output power and spectral purity. The synchronization is attempted using dipolar interactions, which means that the STNOs are fabricated close to each other. For a pair 1 µm apart, it is shown that the synchronization is possible in frequency, whereas the power and linewidth are not significantly improved, meaning that a time domain analysis must be also performed to know the phase-difference role in the process.

Author Keywords. Magnetic tunnel junction, spin torque nano-oscillator, synchronization.

1. Introduction

Magnetic tunnel junctions (MTJs) constituted by two ferromagnetic (FM) layers separated by an MgO nanometric insulating barrier are the ultimate Spintronics device (Zhu and Park 2006). The conjugation of the tunnel magnetoresistance (TMR) effect (Butler 2008) and the manipulation of the magnetization of the free FM layer using a local spin-polarized electric current [spin-transfer torque (STT) effect (Slonczewski 1996; Berger 1996)] makes them candidates to provide a new generation of devices, including non-volatile magnetic memories (Kent and Worledge 2015) and, in this context, spin torque nano-oscillators (STNOs) (Zeng, Finocchio, and Jiang 2013). Nevertheless, the output power and noise levels of a single STNO fall far below those necessary for industrial implementation. As a possible solution, it was proposed to integrate a large number of STNOs in an array. It has been shown that the power is increased by N^2 and the linewidth reduced by N^{-1}, where N is the number of oscillators [up to N=8 (Tsunegi et al. 2018)]. Recently, the synchronization has been experimentally demonstrated mainly by electric mutual synchronization (Tsunegi et al. 2018; Lebrun et al. 2017) and dipolar coupling (Locatelli et al. 2015). While the first one is based on setups not viable for applications (e.g. in (Tsunegi et al. 2018), an individual magnet is needed for each STNO), the second still did not prove experimentally an improvement of power and spectral purity. Here, one aims to achieve synchronization by dipolar coupling by controlling individually the DC current passing through each STNO.

2. Materials and Methods

A 5 Ta / 50 CuN / 5 Ta / 50 CuN / 5 Ta / 5 Ru / 6 IrMn / 2.6 $CoFe_{30}$ / 0.85 Ru / 1.8 $CoFe_{40}B_{20}$ / 1 MgO / 2.0 $CoFe_{40}B_{20}$ / 0.2 Ta / 7 NiFe / 10 Ta / 30 CuN / 7 Ru MTJ stack was deposited by magnetron sputtering (thicknesses in nanometers). Circular pillars (diameter of 350 nm) were defined by e-beam lithography and ion beam milling. The free FM layer (i.e. 2.0 $CoFe_{40}B_{20}$ / 0.2 Ta / 7 NiFe) has a remanent vortex state. Each STNO has an independent top contact (ITC), so that the DC current may be controlled individually. The sustainable oscillation of a single STNO is achieved by applying a sufficiently large DC current and

perpendicular field (Dussaux et al. 2010). The oscillation frequency is tuned by the DC current (Dussaux et al. 2012), so that for a pair of STNOs the synchronization was attempted by maintaining constant the current of one STNO and sweeping the current of the other (Lebrun et al. 2017).

3. Discussion

Figure (a) shows the spectral results obtained for a pair of STNOs (STNO1 and STNO2) 1 µm apart (edge-to-edge distance). Starting with I_{STNO2} = -2.5 mA, each STNO is oscillating individually at a different frequency. As I_{STNO2} is swept, the frequency of STNO2 increases until locking with the frequency of STNO1 (clear for I_{STNO2} = -3.4 mA). Finally, for larger I_{STNO2} values, the oscillations return to the initial behavior. To prove that the frequency locking is a consequence of the interaction between STNOs, Figure (b) shows the frequency of STNO2 when STNO1 is ON (I_{STNO1} = -4.0 mA) and OFF (I_{STNO1} = 0.0 mA). It is clear that the oscillation of STNO1 leads to a frequency shift of STNO2, thus proving the interaction. Nevertheless, the key parameters (i.e. power and linewidth) do not show an effective synchronization. For instance, Figure (c) shows the power of each STNO. In the region where the frequencies are locked (green triangles representing only one peak), the power does not increase significantly, being even lower than the sum of the powers of each peak (green line) where the frequency locking does not exist. This implies that a time domain analysis is required to understand the phenomenon, namely measure the phase difference (Δϕ) between the oscillations of each STNO (Lebrun et al. 2017). For instance, if two STNOs locked in frequency are oscillating in or close to anti-phase (i.e. $\Delta\phi \sim \pi$), the result would be a destructive interference and an expected near zero output power.

3.1. Figures

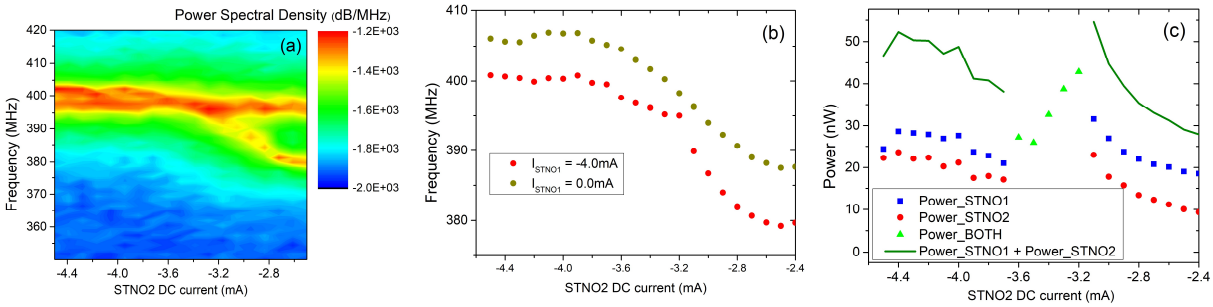

Figure 1: (a) Spectral results obtained for a pair of STNOs, 1 µm apart. The DC current for STNO1 was kept constant (I_{STNO1} = -4.0 mA). (b) STNO2 frequency with STNO1 ON (i.e. I_{STNO1} = -4.0 mA) and OFF (i.e. I_{STNO1} = 0.0 mA). (c) Output power of each STNO obtained from the results shown in (a). In all experiments an external perpendicular field (H_{perp} = 5.3kOe) was applied.

4. Conclusions

Via dipolar interactions, a full synchronization between two vortex-based STNOs (1 µm apart) was attempted. By sweeping the DC current of one of the oscillators, it was possible to induce a frequency locking. The results show that the dynamic behavior of one oscillator depends on the operation of the other (i.e. whether it is OFF or ON). The calculation of fundamental parameters, namely the power, shows an incomplete synchronization, which indicates the need of time domain measurements for a full understanding of the phenomenon.

Acknowledgments
Leandro Martins acknowledges the support of FCT (SFRH/BD/128833/2017).

References

Berger, L. 1996. “Emission of Spin Waves by a Magnetic Multilayer Traversed by a Current.” *Physical Review B* 54: 9353–58. https://doi.org/10.1103/PhysRevB.54.9353.

Butler, William H. 2008. “Tunneling Magnetoresistance from a Symmetry Filtering Effect.” *Science and Technology of Advanced Materials* 9: 014106. https://doi.org/10.1088/1468-6996/9/1/014106.

Dussaux, A., A. V. Khvalkovskiy, P. Bortolotti, J. Grollier, V. Cros, and A. Fert. 2012. “Field Dependence of Spin-Transfer-Induced Vortex Dynamics in the Nonlinear Regime.” *Physical Review B - Condensed Matter and Materials Physics* 86 (1): 1–10. https://doi.org/10.1103/PhysRevB.86.014402.

Dussaux, A, B Georges, J Grollier, V Cros, A V Khvalkovskiy, A Fukushima, H Kubota, et al. 2010. “Large Microwave Generation from Current-Driven Magnetic Vortex Oscillators in Magnetic Tunnel Junctions.” *Nature Communications*. https://doi.org/10.1038/ncomms1006.

Kent, Andrew D, and Daniel C Worledge. 2015. “A New Spin on Magnetic Memories.” *Nature Nanotechnology* 10: 187–91. https://doi.org/10.1038/nnano.2015.24.

Lebrun, R., S. Tsunegi, P. Bortolotti, H. Kubota, A. S. Jenkins, M. Romera, K. Yakushiji, et al. 2017. “Mutual Synchronization of Spin Torque Nano-Oscillators through a Long-Range and Tunable Electrical Coupling Scheme.” *Nature Communications* 8 (May): 15825. https://doi.org/10.1038/ncomms15825.

Locatelli, Nicolas, Abbass Hamadeh, Flavio Abreu Araujo, Anatoly D Belanovsky, Petr N. Skirdkov, Romain Lebrun, Vladimir V Naletov, et al. 2015. “Efficient Synchronization of Dipolarly Coupled Vortex-Based Spin Transfer Nano-Oscillators.” *Scientific Reports* 5: 17039. https://doi.org/10.1038/srep17039.

Slonczewski, J.C. 1996. “Current-Driven Excitation of Magnetic Multilayers.” *Journal of Magnetism and Magnetic Materials* 159: L1–7. https://doi.org/10.1016/0304-8853(96)00062-5.

Tsunegi, Sumito, Tomohiro Taniguchi, Romain Lebrun, Kay Yakushiji, Vincent Cros, Julie Grollier, Akio Fukushima, Shinji Yuasa, and Hitoshi Kubota. 2018. “Scaling up Electrically Synchronized Spin Torque Oscillator Networks.” *Scientific Reports* 8 (1): 13475. https://doi.org/10.1038/s41598-018-31769-9.

Zeng, Zhongming, Giovanni Finocchio, and Hongwen Jiang. 2013. “Spin Transfer Nano-Oscillators.” *Nanoscale* 5: 2219–31. https://doi.org/10.1039/c2nr33407k.

Zhu, Jian-Gang, and Chando Park. 2006. “Magnetic Tunnel Junctions.” *Materials Today* 9: 36–45. https://doi.org/10.1016/S1369-7021(06)71693-5.

Local probe studies on the naturally layered Ca_2MnO_4

Pedro Rocha-Rodrigues[1], Samuel Silva Santos[1], Tiago Leal[1], Gonçalo Nuno Pinho Oliveira[1], Ivan Paula Miranda[2], Ricardo Moreira[1], João Guilherme Correia[3], Lucy Vitoria Credidio Assali[2], Helena Maria Petrilli[2], João Pedro Araujo[1], Armandina Maria Lima Lopes[1]

[1]IFIMUP, Faculdade de Ciências da Universidade do Porto, Rua Campo Alegre, 4169-007 Porto, Portugal.
[2] Instituto de Física - Universidade de São Paulo, Rua do Matão, 1371, 05508-090 Cidade Universitária, São Paulo – Brasil.
[3]C2TN, Instituto Superior Técnico, Universidade de Lisboa, Estrada Nacional 10, ao km 139.7, 2695-066 Bobadela, Portugal.

Abstract
Hyperfine Spectroscopy Perturbed Angular Correlation technique was implemented to study the structural phase diagram of the naturally Layered Perovskite Ca_2MnO_4 at the local scale. By using ^{111m}Cd as the probing isotopes, the measured hyperfine fields, such as Electrical Field Gradient, combined with *ab-initio* calculations, allowed us to study, as a function of temperature, the freezing of MnO_6 octahedral rotations modes that ultimately underlie Ca_2MnO_4 structural phase transitions and its functional property, the uniaxial negative thermal expansion.

Author Keywords. Octahedral Rotations, Hyperfine Spectroscopy, Ruddlesden-Popper phases

Naturally layered perovskites (NLP) such as the Ruddlesden-Popper (R.P.) phases ($Ca_{n+1}Mn_nO3_{n+1}$) have appeared as a fascinating route to achieve nonexpensive room temperature multiferroic materials (Liu et al. 2018). In these NLP, specifically in the $Ca_3Mn_2O_7$ compound, distortions of the lattice such MnO_6 octahedron rotation and tilting modes couple to polar cation dislocation modes inducing a ferroelectric polarization, in a mechanism known as hybrid improper ferroelectricity (Liu et al. 2018). The revived interest in this compound lead us to study the homologous elements belonging to the R.P. series. In particular, Ca_2MnO_4 although non polar presents similar MnO_6 octahedral rotations and, just as $Ca_3Mn_2O_7$, exhibits also the unusual uniaxial negative thermal expansion (Ablitt et al. 2017). Perturbed Angular Correlation γ-γ (PAC) hyperfine technique offers a unique opportunity to probe at the local scale the structural, charge and magnetic phase transitions of these NLP systems (Lopes et al. 2004).

At ISOLDE-CERN, by using metastable ^{111m}Cd isotopes as radioactive probes, PAC measurements were performed in an extensive range of temperatures (1200K - 11K) on the Ca_2MnO_4 compound. Ab-initio electronic structure calculations in the framework of the Density Functional Theory (DFT) were also performed to understand and show how the measured Electrical Field Gradient at the probing sites is sensible to the distinct MnO_6 octahedron distortion modes.

We have measured with high detail, at high temperatures, the structural transition path Ca_2MnO_4 compound takes to achieve the distorted $I4_1/cad$ structural phase. Moreover in the temperature range of 1000K to 10K we only saw evidence for a single local environment, disagreeing with the previously results obtained by transmission electron

microscopy measurements at room temperature conditions that proposed a coexistence of two distinct structural phases *I4$_1$/cad* and *Aba2* (Autret et al. 2004).

Ca_2MnO_4 structural phase diagram was successfully studied at the local scale, the measurement of the Electric Field Gradient by PAC technique allowed to probe accurately the octahedral MnO_6 rotations that underlie the material's structural transitions.

References

Ablitt, Chris, Sarah Craddock, Mark S. Senn, Arash A. Mostofi, and Nicholas C. Bristowe. 2017. "The Origin of Uniaxial Negative Thermal Expansion in Layered Perovskites." *Npj Computational Materials* 3 (1). 44. https://doi.org/10.1038/s41524-017-0040-0.

Autret, C, C Martin, M Hervieu, R Retoux, B Raveau, G Andre, and F Boure. 2004. "Structural Investigation of Ca2MnO4 by Neutron Powder Diffraction and Electron Microscopy" 177:2044–52. https://doi.org/10.1016/j.jssc.2004.02.012.

Liu, Meifeng, Yang Zhang, Ling-fang Lin, Lin Lin, Shengwei Yang, Xiang Li, Yu Wang, et al. 2018. "Direct Observation of Ferroelectricity in Ca3Mn2O7 and Its Prominent Light Absorption Direct Observation of Ferroelectricity in Ca3Mn2O7 and Its Prominent Light Absorption" 22902:3–8. https://doi.org/10.1063/1.5037525.

Lopes, A.M.L, J.P Araújo, E Rita, J.G Correia, V.S Amaral, Y Tomioka, Y Tokura, and R Suryanarayanan. 2004. "Perturbed Angular Correlation Study of Pr1−xCaxMnO3." *Journal of Magnetism and Magnetic Materials* 272–276 (May):E1667–68. https://doi.org/10.1016/j.jmmm.2003.12.957.

Acknowledgments

This work was supported by FCT-Portugal, project Network of Extreme Conditions Laboratories NECL-IFIMUP, NORTE-01-0145-FEDER-022096,IF/00686/2014, POCI-01-0145-FEDER-029454, POCI-01-0145-FEDER-032527 and CERN-FIS-PAR-0005-2017. P.R.R. gratefully thanks the FCT-Portugal for his FCT Grant SFRH/BD/117448/2016.

Local Probing on Ferrolectric $Ca_{n+1}Ti_nO_{3n+1}$ Naturally Layered Perovskite

Tiago Leal[1], Pedro Rocha-Rodrigues[1], Ricardo Moreira[1], Gonçalo N. P. Oliveira[1], João G. Correia[2], João P. Araújo[1], Armandina M. L. Lopes[1]

[1]IFIMUP, Departamento de Física e Astronomia da Faculdade de Ciências da Universidade do Porto, Rua do Campo Alegre, 687, Porto 4769-007, Portugal.
[2]C2TN, Centro de Ciências e Tecnologias Nucleares, Instituto Superior Técnico, Universidade de Lisboa, Estrada Nacional 10, 2695-066 Bobadela LRS, Portugal

Abstract
The Ruddlesden-Popper phase series (R.P.) to which $Ca_3Ti_2O^7$ belongs, have shown very interesting properties such as hybrid improper ferroelectricity (Senn 2015), with the potential development of room temperature multiferroics, uniaxial negative thermal expansion (Senn 2015). The research on R.P. materials is motivated by the potential integration of these into novel technological applications for electronics, data storage or sensing. Time Differential Perturbed Angular Correlation (PAC) at ISOLDE-CERN was performed to characterize the local Electrical Field Gradient of $Ca_3Ti_2O_7$ from 1220K to 10K.

Author Keywords. Hyperfine Interactions, Hybrid Improper Ferroelectric, Ruddlesden Popper Phase Series.

1. Introduction

A key issue in materials science is the search for new multifunctional materials due to their potential applications. The discovery of improper ferroelectrity in artificial superlattices of $SrTiO_3$:$PbTiO_3$ unveiled an approach to design novel ferroelectric materials which lead to an increasing curiosity on similar naturally layered perovskites Ruddlesden-Popper (R.P.) phases. The outstanding physical properties in these systems arises from its lattice distortions.

2. Materials and Methods

In this work, we find $Ca_3Ti_2O_7$, a member of the (RP) series $A_{n+1}B_nO3_{n+1}$, with n=2, having a predicted tetragonal *I4/mmm* structure at higher temperatures that undergoes a structural transition to a orthorhombic structure $A2_1am$ at about ~1035K (Gao 2017). To further investigate this transition, it was used a hyperfine method, in this case, perturbed angular correlation (PAC) spectroscopy.

It was used a local probe of ^{111m}Cd that enabled us to follow octahedral tilt and rotation mechanism responsible for the electronic and structural landscapes and coupled phase transitions. Information on local lattice properties can be extracted by studying the electric field gradient (EFG) tensor. The EFG in the vicinity of the probe atom, which is due to the local charge distribution, allows reconstructing the atomic and electronic environment of the atomic probe in the material. This information can assist in clarifying the origin of the properties exhibited in $Ca_3Ti_2O_7$.

3. Discussion

From the results obtained it's found that there's a change in the V_{zz} and η trend at about the same temperature range as foreseen by electrical resistivity (Liu 2015) and DSC measurements (Gao 2017) for the structural transition, from *I4/mmm* to $A2_1am$, of $Ca_3Ti_2O_7$.

It's also observable that there's no evidence of a mediated structural phase transition differing from the analog compound of $Ca_3Mn_2O_7$, thus agreeing with what was proposed in the literature (Senn 2015, Liu 2015).

With point charge simulations it was confirmed that the ^{111m}Cd probe substitutes the Ca ions at the rocksalt layer site.

4. Conclusions

We were able to observe the $Ca_3Ti_2O_7$ transition that is reported in the literature and find the Ca ion substitution of ^{111m}Cd for PAC measurements. Further studies are required to access the exact transition temperature, evolution of lattice distortions and the second detected local environment.

References

M. S. Senn, A. Bombardi, C. A. Murray, C. Vecchini, A. Scherillo, X. Luo, and S. W. Cheong. 2015. "Negative Thermal Expansion in Hybrid Improper Ferroelectric Ruddlesden-Popper Perovskites by Symmetry Trapping". In Phys. Rev. Lett. 114, 035701

Bin Gao, Fei-Ting Huang, Yazhong Wang, Jae-Wook Kim et al.. 2017. "Interrelation between domain structures and polarization switching in hybrid improper ferroelectric $Ca_3(Mn,Ti)_2O_7$". In Appl. Phys. Lett. 110, 222906

X. Q. Liu, J. W. Wu, X. X. Shi, H. J. Zhao, H. Y. Zhou et al.. 2015. "Hybrid improper ferroelectricity in Ruddlesden-Popper $Ca_3(Ti,Mn)_2O_7$ ceramics". In Appl. Phys. Lett. 106, 202903

Acknowledgments

The authors acknowledge funding from NECL-Network of Extreme Conditions Laboratories under NORTE-01-0145-FEDER-022096, POCI-01-0145-FEDER-029454, CERN/FIS-PAR/0005/2017 and from FCT through EXPL/IF/00686/2014 and FCT for Pedro Rocha-Rodrigues PhD grant SFRH/BD/117448/2016

A multi-grating triboelectric nanogenerator for maritime applications

Cátia Rodrigues[1], Ricardo Esteves[2], Cândido Duarte[2], L. Pessoa[2], André Pereira[1], João Ventura[1]

[1]IFIMUP-IN e Departamento de Física e Astronomia, Faculdade de Ciências, Universidade do Porto, Rua do Campo Alegre, 4169-007 Porto, Portugal
[2]INESC TEC e Departamento de Engenharia Eletrotécnica e de Computadores, Faculdade de Engenharia, Universidade do Porto, Rua Dr. Roberto Frias, 4200-465 PORTO, Portugal

Abstract

Triboelectric nanogenerators (TENGs) are the most viable solution to harvest energy from low-frequency mechanical motions. Here, a triboelectric nanogenerator was developed and implemented inside a floating buoy to harvest the ocean (blue) wave energy. To optimize the TENG, we studied the performance of our device using spheres of different materials. The Nylon spheres generated the largest electrical outputs, so that the number of spheres was also optimized. Thus, a maximum accumulative charge of ~290 nC was generated using 5 Nylon spheres. This optimized device opens new horizons for ways to be integrated in a wide range of buoys and other floating structures, capable of producing energy to power internal sensing devices and other uses.

Keywords. Triboelectric Nanogenerator, Blue Energy, Energy Harvesting, Floating-Buoy

1. Introduction

The world's oceans contain thousands of buoys, floats and other platforms collecting data and others that are not collecting data but that need electrical power for the control system of ballast compensation or fishing feed, mainly used in offshore aquaculture. Traditionally, open ocean buoy are equipped with sensors and electronic systems which have their own battery packs, each one charged by solar panels. However, the power generated by the solar panels have typically a high price, low efficiency and, most important, depends significantly on the illumination conditions. Therefore, novel energy generation solutions that are low cost and scalable and do not depend on the day/night cycle have to be developed to enhance the operation and applicability of wave buoys to obtain truly self-powered conditions. As a solution, triboelectric nanogenerators (TENGs) appeared just in 2012 [1,2] as a powerful mean to generate electrical power from ever present environmental or mechanical motions. TENGs are based on the coupling of the triboelectric effect with electrostatic induction [3,4] and are characterized by high output power densities, low weight, cost-effective materials and highly adaptable designs for different applications [3,4]. Through the repeated contact between triboelectric materials, static charges are created on their surface (with opposite tribo-polarities) due to triboelectrification [5]. The subsequent separation of the triboelectric layers then induces the redistribution of the electrostatic potential, driving the flow of electrons through an external load.

Here, we developed a floating buoy-based triboelectric nanogenerator to harvest mechanical energy in maritime applications. The prototype is composed by a hollow sphere having inside a multi-grating triboelectric nanogenerator and insulator spheres with free movement. When the prototype is used within an ocean scenario, with the water dynamics, energy is generated by the frequent contact of the spheres with the multi-grating TENG.

2. Experimental Results

The floating buoy-based TENG is composed by PTFE spheres (with ~ 12 mm of diameter) and a polydimethylsiloxane film (PMDS; with ~ 220 µm of thickness) as triboelectric materials. This device has six copper electrodes and a substrate of glass epoxy, as shown in Figure 2(a).

The working mechanism of the buoy-based TENG is based on the freestanding mode, in which four major steps are involved [Figure 2(b)]. Under the excitation of a water wave, PTFE spheres roll forth and back between electrodes. After a multiple cycle of contact with the PDMS film, PTFE spheres become negatively charged. When PTFE spheres roll to the right, negative charges are induced on the left electrode. Then, the current flows to the left electrode via the external load to keep the charge balance. When PTFE spheres are overlapped with the electrode, the flow of charges stops and the first half cycle of the FTENG is accomplished. In the same way, when the PTFE spheres roll back, the negative charges flow from the left to the right electrode to induce a reverse current in the load. Then, under the excitation of water waves, PTFE spheres can aleatory roll in the PDMS surface and produce alternating current.

To improve the performance of our TENG, we studied the generated electrical outputs using spheres of different materials, namely, Nylon, polystyrene and PTFE. In accordance with the triboelectric series, Nylon and Polystyrene charge positive and PTFE negatively, in respect to PDMS. Comparing the obtained short-circuit current by the different spheres' material, the Nylon spheres generate the largest signals, as expected from the triboelectric series.

We also studied the dependence of the number of spheres on the generated electrical outputs. In particular, the open-circuit voltage and short-circuit current were measured using 1 to 9 Nylon spheres. No significant differences were obtained in the generated electrical outputs. A maximum accumulative charge of ~ 290 nC in 10 seconds was obtained when using 5 Nylon spheres.

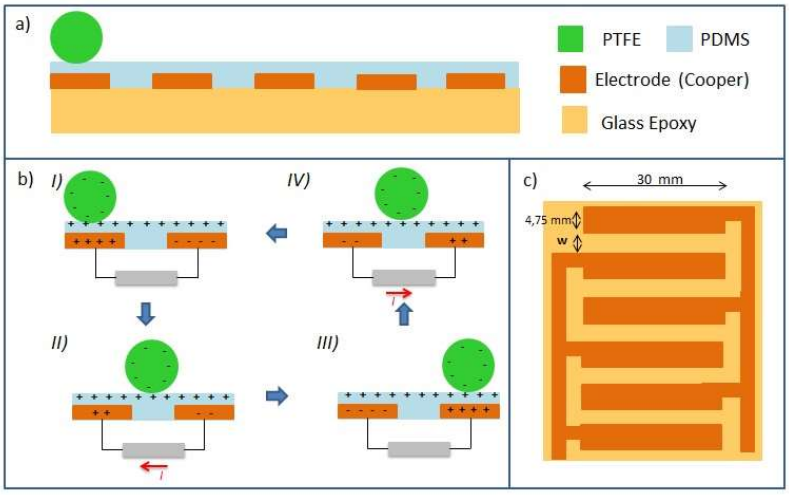

Figure 2: (a) Schematic structure of the multi-grating TENG. (b) Working mechanism of the multi-grating TENG based on the freestanding triboelectric mode. (c) The multi-grating structure of the TENG.

3. Conclusions

In summary, a multi-grating triboelectric nanogenerator was developed and optimized to be implemented within a floating buoy. In relation to the TENG, spheres of different

materials with different tribo-polarities (based on typical triboelectric series) were tested to improve the performance of our TENG and the largest electrical outputs were obtained using Nylon spheres. Also, the influence of spheres' number on TENG performance was studied, giving an optimum number of five Nylon spheres. The design of our TENG provides an innovative and effective approach toward blue energy harvesting by connecting more grating TENG to form a multi-TENG.

References

[1] Wang, Z. L., T. Jiang, L. Xu. 2017. *"Toward the blue energy dream by triboelectric nanogenerator networks". Nano Energy,* 39: 9-23. DOI: 10.1016/j.nanoen.2017.06.035

[2] Yang, X., S. Chan, L. Wang, W. A. Daoud. 2018. "*Water tank triboelectric nanogenerator for efficient harvesting of water wave energy over a broad frequency range*". *Nano Energy*, 44: 388-398. DOI: 10.1016/j.nanoen.2017.12.025

[3] Z. L. Wang. 2019.*"Entropy theory of distributed energy for internet of things"*. *Nano Energy*, 58: 669-672. DOI: 10.1016/j.nanoen.2019.02.012

[4] Rodrigues, C., C. Alves, J. Puga, A. Pereira, J. Ventura. 2016. *"Triboelectric driven turbine to generate electricity from the motion of water". Nano Energy*, 30: 379-386. DOI: 10.1016/j.nanoen.2016.09.038

[5] Seol, M., S. Kim, Y. Cho, K. E. Byun, H. Kim, J. Kim, S. K. Kim, S. W. Kim, H. J. Shin, S. Park. 2018*. "Triboelectric Series of 2D Layered Materials". Advanced Materials*, 30 (39). DOI: 10.1002/adma.201801210

Acknowledgments

The authors acknowledge funding from FEDER and ON2 through project Norte-070124-FEDER-000070, NECL - NORTE-01-0145-FEDER-022096 from FCT through the Associated Laboratory - IN. This work was funded through projects FA 02 2017 002, UID/NAN/50024/2019, UTAP-EXPL/NTec/0021/2017 and POCI-01-0145-FEDER-028766 from Fundação para a Ciência e Tecnologia (FCT), Portugal. The authors also acknowledge support from the International Consortium of Nanotechnologies (ICON) funded by Lloyd's Register Foundation, a charitable foundation which helps to protect life and property by supporting engineering-related education, public engagement and the application of research. J. V. acknowledges financial support through FSE/POPH and project PTDC/CTM-NAN/3146/2014. C. Rodrigues acknowledges project UTAP-EXPL/NTec/0021/2017 for a research grant.

Wearable Textile Supercapacitor based on Nitrogen-doped Carbon Nanomaterial

Rui S. Costa[1], André M. Pereira[2], Clara Pereira[1]

[1] REQUIMTE/LAQV, Chemistry and Biochemistry Department, Faculty of Sciences, University of Porto, Rua do Campo Alegre s/n, 4169-007 Porto, Portugal
[2] IFIMUP-IN, Physics and Astronomy Department, Faculty of Sciences, University of Porto, Rua do Campo Alegre s/n, 4169-007 Porto, Portugal.

Abstract

This work reports on the fabrication of flexible textile supercapacitors (FTSCs) based on undoped and nitrogen-doped carbon nanomaterial (N-CNM) coated textile electrodes and a solid-gel electrolyte. Fabrics were firstly coated with the undoped and N-CNM materials to fabricate the textile electrodes. The incorporation of the nanomaterials was confirmed by X-ray diffraction and scanning electron microscopy. The FTSCs were then produced through the assembly of two textile electrodes coated with CNM or N-CNM, separated by a solid-gel electrolyte. The electrochemical performance evaluation revealed that the FTSC based on N-CNM exhibited 52% higher specific capacitance than that based on the undoped CNM (13.85 F g^{-1} *vs.* 7.87 F g^{-1}), delivering an energy density of 8.89 W h kg^{-1} and a power density of 0.47 kW kg^{-1}. The FTSCs allowed supplying low power consumption systems, such as LEDs and a temperature sensor, confirming their energy storage efficiency and stability.

Author Keywords. Wearable Supercapacitors, N-doped Carbon Nanomaterials, Textiles, Solid-gel Electrolyte.

1. Introduction

The increasing evolution of smart textiles, which need flexible energy storage systems, has aroused the interest on developing textile supercapacitors (SCs) to power wearable electronics, printable electronics and smart textiles [1]. SCs are an attractive technology to store energy, which allows narrowing the gap between batteries and electrolytic capacitors in terms of power density and energy density. This gap reduction is possible due to the unique characteristics of SCs, such as the ability to store energy, fast charging, long lifetime (>10 000 cycles) and high power density [2]. However, their energy density is still limited, which prevents them from being used for high energy consumption devices. To improve the energy density of SCs, N-doped carbon nanomaterials (CNMs) have shown to be promising electrode materials, since the nitrogen based functionalities impart pseudocapacitive properties. In this sense they can increase the capacitance of the SCs, without losing the high power density [3].

2. Discussion

To produce the FTSCs, 4×4 cm^2 textile substrates were coated with CNM and N-CNM. The amount of incorporated nanomaterials on the resulting textile electrodes was 10.31 and 4.35 wt% for the textile coated with CNM and N-CNM, respectively. In addition, the textile coated with CNM presented higher electrical resistance than the textile coated with N-CNM. The produced FTSCs were electrochemically characterized by cyclic voltammetry (CV), galvanostatic charge/discharge (GCD) method and electrochemical impedance spectroscopy (EIS). The N-CNM and CNM based FTSCs exhibited equivalent series resistance (R_{ESR}) of 317.72 and 88.77 Ω (Figure 3A), specific capacitance (C_T) values of 13.85 and 7.87 F g^{-1} and an operating voltage (V_0) of 2.15 and 2.39 V, respectively. The presence of the N-containing groups in N-CNM allowed increasing the C_T of the resulting FTSC in 52% (Figure 3B). Moreover, the N-CNM based FTSC showed an energy density (E) of 8.89 W h

kg^{-1} at 0.47 kW kg^{-1} power density (*P*), which was 2 times higher than the energy density of the CNM based FTSC (5.39 W h kg^{-1} at 1.67 kW kg^{-1}).

Finally, both FTSCs allowed powering electronic devices, such as LEDs or a temperature sensor for more than 2 and 5 mins, respectively.

2.1. Figures

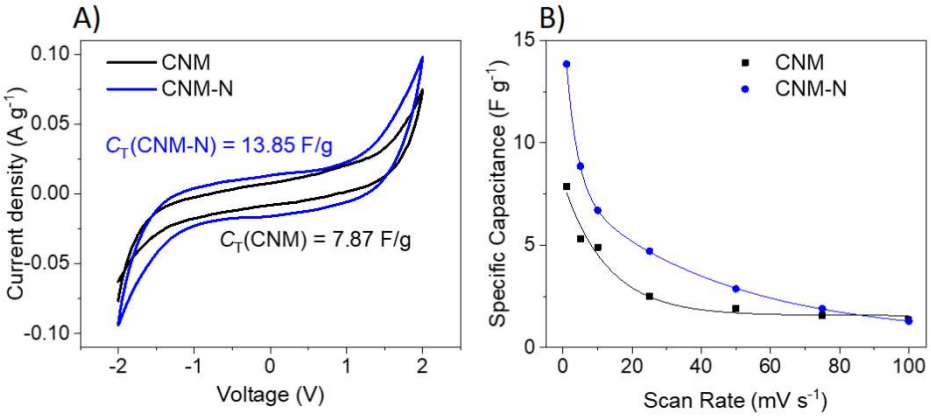

Figure 3: A) *i-V* cycles and specific capacitance values at 1 mV s^{-1} of CNM and CNM-N based FTSCs. B) Specific capacitance of CNM and CNM-N based FTSCs as a function of the scan rate.

3. Conclusions

In summary, efficiently all-solid-state FTSCs were directly produced on fabrics (cotton substrate) using a cost-effective process implemented in the Textile Industry. The doping of the CNM with nitrogen heteroatom showed to be a promising strategy to enhance the energy density of the FTSCs, with only a slight decrease of the power density.

References

[1] M. Jian, C. Wang, Q. Wang, H. Wang, K. Xia, Z. Yin, M. Zhang, X. Liang, Y. Zhang, Advanced carbon materials for flexible and wearable sensors, Sci. China Mater. 60 (2017) 1026–1062. doi:10.1007/s40843-017-9077-x.

[2] A. González, E. Goikolea, J.A. Barrena, R. Mysyk, Review on supercapacitors: Technologies and materials, Renew. Sustain. Energy Rev. 58 (2016) 1189–1206. doi:10.1016/j.rser.2015.12.249.

[3] Y. Deng, Y. Xie, K. Zou, X. Ji, Review on recent advances in nitrogen-doped carbons: preparations and applications in supercapacitors, J. Mater. Chem. A. 4 (2016) 1144–1173. doi:10.1039/C5TA08620E.

Acknowledgments

This work was funded by FEDER - European Regional Development Fund through COMPETE 2020 - POCI and by Portuguese funds through FCT/MCTES under Program PT2020 in the framework of the projects PTDC/CTM-TEX/31271/2017, UID/QUI/50006/2019 and UID/NAN/50024/2013. R.S.C. thanks UniRCell Project (POCI-01-0145-FEDER-016422) for a MSc. grant. C.P. thanks FCT for the FCT Investigator contract IF/01080/2015.

Solid-state batteries with ferroelectric electrolyte and polymer composites

Rita Carvalho Veloso[1*], Joana Espain Oliveira[1], Maria Helena Braga[1]

[1] Physics Engineering Department, Faculty of Engineering, University of Porto
Rua Dr. Roberto Frias s/n 4200-465 Porto, Portugal rveloso@fe.up.pt.

Abstract

It is necessary to reduce the dependence of modern society on fossil fuels. To achieve this, it is mandatory to create strategies to store electric power from other renewable sources, such as solar and wind energy. Solid-state batteries are a new safe format of energy storage that can satisfy those needs, in contrast with the lithium-ion batteries, which are flammable due to the liquid electrolyte[1].

We analyze the performance of a solid electrolyte, which is a ferroelectric material with remarkable properties such as high dielectric constant and ionic conductivity comparable to that of liquid electrolyte[2]. Although its dielectric constant is extremely high, we have developed strategies to further increase the electrolyte's polarization increasing the stored charge. This strategy involves mixing with polymer matrices with good ionic conductivity, high chemical stability, low cost and safety[3]. In this paper, we present results of such mixtures and heating cycles.

Author Keywords: Solid State Batteries; Solid Electrolyte; Ferroelectric Electrolyte

1. Introduction

The batteries that were invented in the 80's use liquid electrolytes to carry the lithium ions between the anode and the cathode. If a battery cell is charged too quickly, it can cause dendrites, causing a short circuit that can lead to explosions and fires. The flammability and leakage of liquid electrolyte batteries greatly limited the safe application and led to the development of solid-state batteries[1]. Our solid-state batteries use a solid electrolyte that as extraordinary properties like an extremely high dielectric constant (> 10^6) and ionic conductivity ($o > 10^{-2} Scm^{-1}$ at 25 °C)[2].

Low cost A-glasses (A=Li or Na) are easily prepared and offer a safe rechargeable battery cell with high energy density and a fast charge. They also allow plating of an alkali-metal anode without dendrites4.

2. Strategies and Methods

We have started by mixing the Na^+ glass electrolyte[4] with different polymeric matrices and assembled the battery system[3]. The properties of these batteries are measured by Electrochemical Impedance Spectroscopy (EIS) and Cyclic Voltammetry (CV). The goal was to analyze how internal resistance changes after changing certain parameters like, for example, the temperature and to analyze the possible redox reactions occurring in the electrodes (metal) while charging and discharging. These tests can show the remnant polarization, electrochemical potentials difference between electrodes and electrode and electrolyte.

3. Results

Here, we show the results obtained by EIS and CV of different mixtures with polymeric matrices and electrolyte, at room temperature and after heating in the furnace. We can observe by EIS how the internal resistance of the electrolyte changes after the heating cycles. It was possible to determine that in both cases there is a decrease in the internal resistance (Figure 1). Cyclic Voltammetry shows maximum current flow for system with the polymer matrix 1 and electrolyte mixture (Figure 2).

3.*1. Figures*

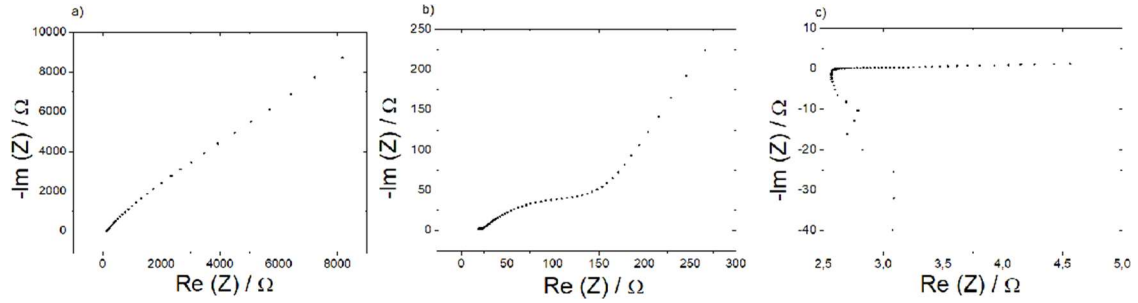

Figure 1: Electrochemical Impedance Spectroscopy of the solid electrolyte (a) at room temperature, the mixture with polymer 1 at room temperature (b) and after heating in the furnace at 76°C (c).

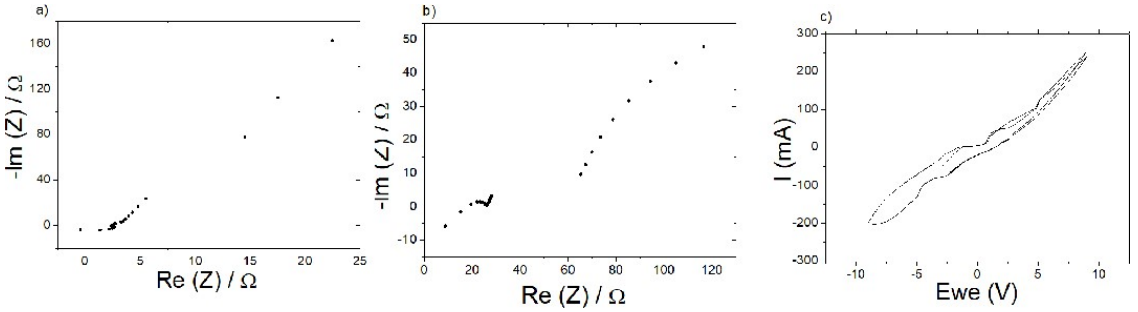

Figure 2: Electrochemical Impedance Spectroscopy of the mixture with polymer 2 at room temperature (a) and after heating in the furnace at 100°C (b). Cyclic Voltammetry for mixture with polymer 2 (sample area: 2,5 x 2,5 cm) from -10V to 10V with a scan rate of 100 mVs^{-1} (c).

References

[1] Braga, M.H., Grundish, N.S., Murchinson, A.J., Goodenough, J.B. 2017. "Alternative strategy for safe rechargeable battery". *Energy & Environmental Science* 10: 331-336. Accessed 24 May 2019 DOI: 10.1039/C6EE02888H;

[2] Braga, M.H., Oliveira, J.E., Kai, T., Murchison, A.J., Bard, A.J., Goodenough, J.B. 2018. "Extraordinary dielectric properties at heterojunctions of amorphous ferroelectrics" *Journal of the American Chemical Society* 14 (51): 17968-17976. Accessed 24 May 2019 DOI:10.1021/jacs.8b09603;

[3] Arya, A., Sharma A.L. 2017. "Polymer electrolytes for lithium ion batteries: a critical study". *Ionics* 23 (3): 497540. Accessed 24 May 2019 DOI: 10.1007/s11581-016-1908-6;

[4] Braga, M.H., Ferreira, J.A., Murchison, A.J., Goodenough, J.B. 2017. "Electric Dipoles and Ionic Conductivity in a Na^+ Glass Electrolyte". *Journal of The Electrochemical Society*, 164 (2) A207-A213. Accessed 24 May 2019 DOI: 10.1149/2.0691702jes;

[5] Braga, M.H., Murchison, A.J., Ferreira, J.A., Singhb, P., Goodenough, J.B. 2016 "Glass-amorphous alkali-ion solid electrolytes and their performance in symmetrical cells" *Energy & Environmental Science*, 9, 948-954. Accessed 24 May 2019 DOI: 10.1039/C5EE02924D;

Acknowledgments

We thank the FCT and Compete 2020 for financial support through PTDC/CTM-ENE/2391/2014 - POCI-01-0145-FEDER-016854. RSC thanks to Project (POCI-01-0145-FEDER-016854) for MSc. Grant.

Optical analogues of superfluids in Nematic Liquid Crystals

Tiago D. Ferreira[1,2], Nuno A. Silva[1,2] and Ariel Guerreiro[1,2]

[1] Department of Physics and Astronomy, Faculty of Sciences, University of Porto, R. Campo Alegre, 4169-007, Porto, Portugal

[2] INESC TEC - CAP, R. Campo Alegre, 4169-007, Porto, Portugal

Abstract

Light propagating in a nematic liquid crystal can be interpreted as fluid where the interaction between the photons is mediated through the nonlocal nonlinearity. The similarities that exist between the model used to describe this system and others with superfluid effects suggest the possibility of having a superfluid-like behavior of light in nematic liquid crystal. In this work, we explore this possibility by studying the drag-force cancelation effect, which constitutes a direct manifestation of the superfluid regime.

Author Keywords. Optical analogues, Superfluidity, Nematic Liquid Crystals, Drag-Force, Schrödinger-Newton equation, GPGPU supercomputing

1. Introduction

In the past years, the field of Physics has seen a growing interest in physical systems that share a similar mathematical description. The interest relies on the possibility of using one of these systems to emulate phenomena of the others and this constitutes what is commonly known as physical simulations or optical analogues. The Schrödinger-Newton system is one of such systems since it can describe gravitational (Roger 2016) and superfluid phenomena, which are difficult or even impossible to study under controlled conditions, as well as light propagating in Nematic Liquid Crystals (NLCs), a system that it is easily implemented in an experiment. NLCs can indeed emulate fluids with light and support superfluid phenomena (Ferreira 2018), and in this work we demonstrate a direct manifestation of this effect by studying the cancellation of the drag-force when the light fluid encounters an obstacle in the medium.

2. Methods and Discussion

NLCs (Alberucci 2014) are composed by a liquid and organic molecules that, in the nematic phase, tend to align along a certain direction. The relation between the direction of these molecules and the polarization of the electric field dictates the distribution of the refractive index. Under the paraxial approximation the system can be modeled as

$$i\frac{\partial E}{\partial z}+\frac{1}{2}\frac{d^2E}{dx^2}-2\theta E=0, \quad (1)$$

$$\nu\frac{d^2\theta}{dx^2}-2q\theta=-2|E|^2, \quad (2)$$

where E is the envelope of the electric field and θ is the deviation of the direction of the molecules due to the presence of the electric field. The constants ν and q are parameters that characterize the NLCs. The fluid interpretation of light propagating in NLCs arises from the transformation of equations 1 and 2 into a set of hydrodynamic equations through the Madelung transformation (Ferreira 2018). From this interpretation, it is possible to establish the existence of a critical velocity below which the light fluid behaves as a superfluid, i.e. it moves as if it had no viscosity (Ferreira 2018). One way to verify the existence of this regime is through the study of the force that the fluid exerts on an obstacle that is present in the medium. In the superfluid regime, this force is expected to be null since there is no diffraction in the transverse plane due to the defect. Consequently, the linear momentum is also expected to be null. To demonstrate this effect, we constructed and simulated an all-optical experiment, Figure 2-A, where a small Gaussian beam and a plane wave are used to create the defect and the fluid of light in the medium, respectively. By varying the angle at

which the plane wave enters the medium we can control the velocity of the fluid and thus probe the system for velocities above and below the critical speed. To quantify the drag-force effect we studied the force that the fluid exerts on the obstacle and the linear momentum of the perturbations generated on the fluid. Both quantities are measured in the transverse plane. Figure 2-B shows that for a fluid velocity below the critical speed, the force of the fluid on the defect tends to zero after a transient regime, while for a fluid velocity larger than the critical speed the force is not null. Furthermore, the linear momentum, Figure 2-C, of the perturbations generated on the fluid are approximately zero below the critical velocity, and above this value, it grows until it reaches a maximum value and then starts to decrease. These results, although preliminary, suggest the possibility of generating a superfluid regime in nematic liquid crystals.

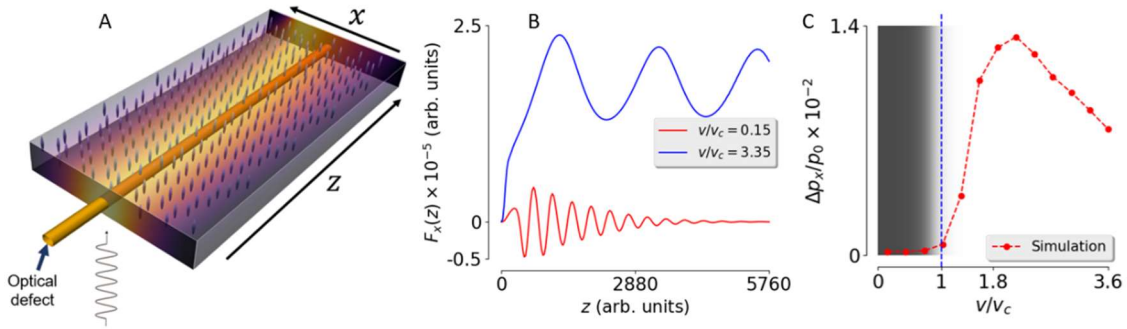

Figure 1: Drag-force cancellation in NLCs results. A schematic representation of the experiment to probe the superfluidic behavior in nematic liquid crystals. B - Force exerted by the fluid on the obstacle for velocities above and below the critical velocity. C - Normalized momentum variation along the x direction for different fluid velocities.

3. Conclusions

Optical analogues are an interesting way do study phenomena under controlled conditions that otherwise would be hard or even impossible to study. The Schrödinger-Newton model can be emulated with NLCs and these are an interesting system to develop and implement optical analogues. In this work, we showed a direct manifestation of superfluid effects with NLCs and observed the drag-force cancellation characteristic of this regime.

References

Ferreira, T. D., Silva, N. A., and Guerreiro, A., **"**Superfluidity of light in nematic liquid crystals," Physical Review A 98, 023825 (Aug 2018).

Roger, T., Maitland, C., Wilson, K., Westerberg, N., Vocke, D., Wright, E. M., and Faccio, D., "Optical analogues of the newton-schrödinger equation and boson star evolution," Nature Communications 7(13492) (2016).

Alberucci, A., Assanto, G., Michael, J., MacNeil, L., and Smyth, N. F., "Nematic liquid crystals: An excellent playground for nonlocal nonlinear light localization in soft matter," Journal of Nonlinear Optical Physics & Materials 23(4), 1450046 (2014).

Acknowledgments

This work is supported by the ERDF - European Regional Development Fund through the Operational Programme for Competitiveness and Internationalisation - COMPETE 2020 Programme and by National Funds through the Portuguese funding agency, FCT - Fundação para a Ciência e a Tecnologia within project <<POCI-01-0145-FEDER-032257>>

Non-Destructive Testing Using Advanced Magnetorheological Elastomers

J. A. Silva[1], C. Gouveia[2], G. Dinis[2], H. Araújo[2], A. M. Pereira[1]

[1] IFIMUP and IN – Institute of Nanoscience and Nanotechnology, Departamento de Física e Astronomia, Faculdade de Ciências, Universidade do Porto, 4169-007 Porto, Portugal
[2] EQS Global, Rua Joaquim Dias Rocha, n.º 354 Zona Industrial da Maia 1, sector X, 4470-211 Maia, Portugal

Abstract

Regular inspection of petrochemical, nuclear and electrical power generation facilities is critical to ensure safety and avoid health and environmental issues. The periodic evaluation of the integrity of these infrastructures requires non-destructive evaluation (NDE) as well as equipment that can withstand demanding conditions (e.g. high temperatures, corrosive ground, etc).
Magnetostrictive materials have become an important transduction tool to use in NDT of corrosion and defects in pipelines. FeCo is one of the most cost-efficient magnetostrictive materials, as it has a large magnetostrictive coefficient and is cheap compared with rare-earth based ferromagnets while offering competitive advantages over its piezoelectric and optical counterparts. FeCo is usually fabricated in sheets and rods but is too brittle to be worked and applied in the field of monitoring. To overcome this issue, we report the fabrication of a FeCo-resin composite, known as a magnetorheological elastomer. Besides the magnetostrictive Fe-Co, Fe_3O_4, $MnFe_2O_4$ and $Y_3Fe_5O_{12}$ were also explored. The magnetorheological elastomer herein studied is composed of magnetic particles and a binding paste, produced with PVA or PVDF. The obtained thick films (around 200 μm) show magnetic behavior, as well as mechanical flexibility. Characterization results are presented, including morphological, atomic and magnetic analysis, such as SEM, XRD and VSM. A holistic solution for non-destructive pipe testing involving a magnetorheological stripe is presented.

Author Keywords. Magnetostriction, magnetorheological elastomer, non-destructive testing, particle synthesis, ink formulation.

Introduction

Pipelines in refineries and power plants are constantly subject to corrosion and cracking and require periodic inspection. The technological revolution has allowed the increasing inspection and monitoring of these assets, to ensure better safety standards. Acoustic waves are used for this purpose and are generated using magnetostricitive materials. The principle of operation of a magnetostrictive transducer requires two orthogonal magnetic fields to produce a torsional wave (Wiedemann effect), provided one of them is static and the other is time varying. The shape variation in the transducer transmits an acoustic wave to the adjacent material (pipe) that will propagate until reaching a blockage (crack or edge). The reflection is detected by the transducer which allows the determination of the distance to the blockage.

The large size of these devices can compromise the versatility and efficiency because of the reduced interface contact. Moreover, such inspection tools are typically expensive and are not designed for the permanent monitoring of individual pipes. Due to the absence of a fully integrated electronic system, the inspection of the structural integrity of the pipelines remains a costly solution that could benefit from further technological improvements. In this work, we intend to produce a flexible printed system, both versatile and low-cost, while showing the large potential of this approach in further technological applications.

The composite will consist of magnetic particles embedded in a polymeric matrix, the so-called magnetorheological elastomer. Different materials, shapes and sizes will be used in order to optimize the magnetostrictive-like response of the composite. The polymer matrix ensures large flexibility as well as electric insulation of the composite, which are key characteristics for the good performance of the acoustic transducer. The advantages of using magnetorheological elastomers include reduced costs, and higher stress and strain failure.

This transducer will be coupled to two orthogonal inductive coil systems that stimulate and sense the magnetic response caused be the acoustic waves. The inductive coils will be fabricated using printing methods, where the flexibility, size, shape and number of turns are key aspects to improve their performance.

Materials and Processes

In this work we fabricated and optimized magnetorheological elastomers. We have produced different magnetic particles: Fe50Co50, Y3Fe5O12, Fe3O4 and MnFe2O4. The magnetic particles were individually prepared using different synthesis methods, namely polyol (Fe50Co50), sol-gel (Y3Fe5O12) and coprecipitation processes (Fe3O4 and MnFe2O4). These particles were then embedded in PVA and PVDF polymeric matrices, at different concentrations. The embedding process occurs via the formulation of inks, using the magnetic particles, polymer and the respective solvent. They are further processed using printing techniques, such as stencil and screen-printing.

Morphological, crystallographic and magnetic characterization was performed on the fabricated samples. Moreover, laboratorial measurements enabled the determination of the magnetic response of the magnetorheological composite.

Discussion

The synthesis process of the magnetic particles was optimized for each material. An EDS analysis allowed us to conclude that the optimized process yields particles with the expected stoichiometry. Also, magnetic studies were performed to evaluate the magnetic behaviour of the particles (ferromagnetism, ferrimagnetism, superparamagnetism).

Regarding the magnetorheological elastomers, Scanning Electron Microscopy (SEM) analysis was performed, complemented by X-ray Diffraction (XRD) that will provide crystallographic information, as well as the crystallite sizes. We can also conclude that the particles have a good dispersion throughout the polymeric matrix through the SEM analysis. Preliminary flexibility tests of different composites will help us determine the next steps for this investigation.

Conclusion

We have synthesized and optimized ferromagnetic, ferrimagnetic and superparamagnetic particles. The magnetic particles were used in the formulation of magnetostrictive inks, using different polymers and solvents. The inks were processed with stencil and screen-printing techniques, resulting in a magnetorheological elastomer. The different composites were characterized and tested at laboratorial scale. In the future, we intend to develop a less expensive, more efficient, flexible and scalable solution for the monitoring of pipelines and other critical assets.

Fabry-Pérot interferometer fabricated in fused silica through femtosecond laser micromachining

João M. Maia[1,2], Vítor A. Amorim[1,2], Duarte Viveiros[1,2], P. V. S. Marques[1,2]

[1]CAP – Centre for Applied Photonics, INESC TEC, Rua do Campo Alegre 687, 4169-007 PORTO, Portugal (joao.m.maia@inesctec.pt) ORCID 0000-0001-9260-4247 (vitor.a.amorim@inesctec.pt) ORCID 0000-0002-2173-2441 (carlos.d.viveiros@inesctec.pt) ORCID 0000-0003-0674-9963

[2]Department of Physics and Astronomy, Faculty of Sciences, University of Porto, Rua do Campo Alegre 4169-007 PORTO, Portugal (psmarque@fc.up.pt) ORCID 0000-0002-3709-1968

Abstract

A Fabry-Pérot interferometer was fabricated inside a fused silica substrate through femtosecond laser micromachining. The influence of the waveguide's writing parameters on the quality of the measured signal was studied for an interferometer with a 27-µm wide cavity. Optimal signal-to-noise ratio and fringe visibility were obtained for waveguides written at 75 nJ and 50 µm/s. The device was then tested as a refractive index sensor, exhibiting a maximum sensitivity of 1181.4±23.6 nm/RIU in the index range of 1.2962 to 1.3828 (at 1550 nm).

Author Keywords. Fabry-Pérot interferometer, femtosecond laser micromachining, optical sensing.

1. Introduction

Femtosecond (fs) laser micromachining is a high precision fabrication technique that can be used to write three-dimensional structures for applications in photonics or microfluidics, among others (Choudhury 2014). Infused silica, the laser-induced modification, started by a non-linear light absorption process, can lead to: (i) an increase of the refractive index around the focal volume that allows the formation of optical circuits, or (ii) an increase of the etch rate of the laser-affected zones relative to the bulk material, leading to an anisotropic HF (hydrofluoric acid) etching reaction that enables the fabrication of microfluidic systems.

Several devices, which combine both types of structures, have already been demonstrated for cell trapping and optical sensing, thereby demonstrating the potential of this technique in the design of true lab-on-a-chip devices. Here, we develop a Fabry-Pérot interferometer, which is formed by an optical waveguide that is written orthogonally to a microfluidic channel (Fig. 1a). The device can be used as an optical sensor, where the sensitivity to variations in the refractive index of the medium inside the cavity arises from the ensuing change of the optical path difference between both interfering beams. The influence of the waveguide's writing parameters on the spectrum's signal-to-noise ratio (SNR) and visibility was analyzed, and the response of the interferometer to refractive index variations was determined.

2. Materials and Methods

A fiber amplified fs-laser system emitting a second harmonic beam at 515 nm with an approximate pulse duration of 250 fs at 500 kHz was used to fabricate the device. The laser beam was focused inside a fused silica substrate (Suprasil 1) with a 0.55 numerical aperture aspherical lens mounted in a vertical piezostage. The substrate was mounted on X-Y air-bearing linear stages and translated in relation to the beam focus. The optical waveguide and microfluidic channel were written sequentially to guarantee perfect alignment between both.

Several 1.3-cm long waveguides were written 55 µm below the silica surface with pulse energies and scanning speeds between 50 and 200 nJ and 50 and 400 µm/s, respectively, and with the polarization of the laser beam set parallel to the writing direction. The microfluidic channel was written from the bottom to the top by stacking multiple adjacent modification tracks with a horizontal and vertical spacing of 2 and 3 µm respectively, at a speed of 500 µm/s, pulse energy of 80 nJ and with the beam's polarization perpendicular to the scanning direction. Wet etching was done afterwards in an ultrasonic cleaner by immersing the substrate in a 10% HF solution for 105 minutes. The channel has a final width and depth of 27 and 90 µm, respectively. Albeit the channel's sidewall has a low surface roughness, it is deviated 5° from the vertical, utmost, due to the finite HF etching selectivity.

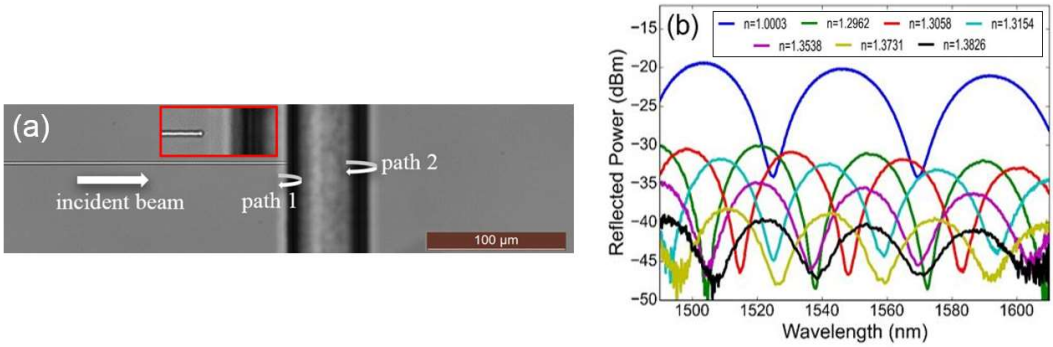

Figure 4: (a) Top-view image of the Fabry-Pérot interferometer. (b) Measured spectra of an interferometer with the waveguide written at 75 nJ and 50 µm/s.

3. Results and Conclusion

From the gathered spectra, we observed that the waveguide's writing parameters influence the quality of the signal. Waveguides written with higher pulse energies revealed a lower SNR due to the existence of inhomogeneities within the waveguide, which lead to random reflections and cause arbitrary power fluctuations in the measured spectrum. Visibility is also enhanced when writing at lower scanning speeds, due to both the waveguide's higher numerical aperture and the channel's vertical deviation. Both the SNR and fringe visibility were found optimal for waveguides written with 75 nJ at 50 µm/s (Fig. 1b). We tested an interferometer, with the waveguide written with the latter parameters, as a refractive index sensor and obtained a linear response in the refractive index range 1.2962 to 1.3828 (at 1550 nm). A maximum sensitivity of 1181.4±23.6 nm/RIU was determined, corresponding to a minimum resolvable index variation of 8.5×10-4.

References

Choudhury, D., J. R. Macdonald and A. K. Kar. 2014. "Ultrafast laser inscription: Perspectives in future integrated applications". *Laser and Photonics Review* 8 (6):827-846. DOI: 10.1002/lpor.201300195.

Acknowledgments

This work was supported by Fundação para a Ciência e Tecnologia through grant no. SFRH/BD/133095/2017. The results presented in this paper are part of the Project "On Chip Whispering Gallery Mode Optical Microcavities For Emerging Microcontaminant Determination in Waters" – SAFE WATER, supported and co-founded by the European Commission, Directorate-General Communications Networks, Content and Technology (DG CONNECT) under the ERA-NET Cofund scheme – Horizon 2020 "Horizon 2020 – the Framework Programme for Research and Innovation (2014-2020)".

Low-loss broadband femtosecond laser written surface waveguides for enhanced evanescent coupling

Vítor A. Amorim[1,2], João M. Maia[1,2], D. Viveiros[1,2], P. V. S. Marques[1,2]

[1] Centre for Applied Photonics, INESC TEC, Rua do Campo Alegre 687, 4169-007 Porto, Portugal
[2] Department of Physics and Astronomy, Faculty of Sciences, University of Porto, Rua do Campo Alegre 4169-007 Porto, Portugal

Abstract

The fabrication of low-loss broadband optical waveguides with femtosecond laser direct writing is reported in Eagle2000. The influence of typical fabrication parameters on the waveguide's spectral characteristics is explored from 500 to 1700 nm. Optimal results were achieved for very high scanning velocities (≈10 cm/s), reducing fabrication times and allowing the mass fabrication of devices employing such optical platforms. The suitability of such waveguides to be brought to the surface, through wet etching, for enhanced evanescent coupling with the external dielectric medium was also explored, since this serves as a gateway to produce optical sensors. The small etch selectivity allowed the placement of the guiding region as close to the substrate's surface as required.

Author Keywords. Eagle2000, femtosecond laser direct writing, low-loss broadband surface waveguides.

1. Introduction

Femtosecond laser direct writing is a fabrication technique that relies on a very localized modification to manufacture three-dimensional structures. In several materials, the modification translates into an increased refractive index, enabling the fabrication of optical circuits. However, the spectral characteristics of such optical waveguides are far from ideal (Amorim 2019). Furthermore, exposing the light guided in optical waveguides to the surface is of great interest in sensing applications. Ablation sets a limit on how shallow a waveguide can be, so, in this work, we use the femtosecond laser direct writing technique and wet etching for the fabrication of low-loss broadband surface waveguides in Eagle2000 substrates.

2. Materials and Methods

The materials and methods used in this work are described in (Amorim 2019). In this work the glass is Eagle2000 and the repetition rate of the laser was set to 1 MHz.

3. Experimental Results and Discussion

The insertion losses of 2.5 cm long optical waveguides inscribed in Eagle2000 with varying pulse energy and scan velocity were measured, as depicted at the top of figure 1. Here, an increase in insertion loss is visible whenever the wavelength decreases or increases from a certain position. It also depends on the fabrication parameters, presenting two distinct behaviors at shorter and longer wavelengths. Longer wavelengths display smaller insertion losses as pulse energy increases, increasing as scan velocity increases. Shorter wavelengths exhibit a decrease in insertion loss for higher pulse energy and scan velocity.

The suitability of exposing such waveguides to the surface was also explored through wet etching, since this serves as a gateway to produce optical sensors. The result, after hydrofluoric acid etching, is displayed at the bottom left of figure 1. As can be seen, the small etch selectivity allowed the placement of the guiding region as close to the substrate's

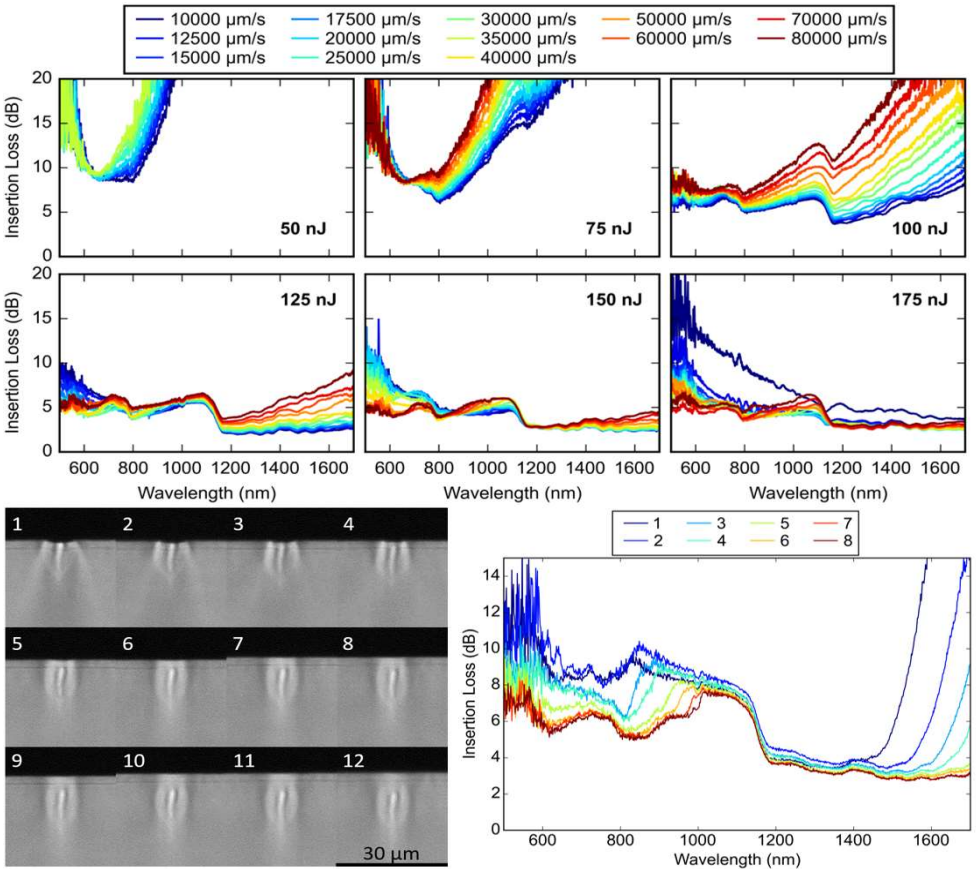

Figure 5: (Top) Insertion loss of 2.5 cm long optical waveguides inscribed in Eagle2000 for varying pulse energy and scan velocity. (Bottom Left) Cross-sectional images of the optical waveguides etched to the surface. (Bottom Right) Insertion loss of the optical waveguides etched to the surface.

surface as required, enabling the tuning of the evanescent field coupling to the exterior, while retaining their general spectral characteristics (bottom right of figure 1).

4. Conclusions

The fabrication of low-loss broadband optical waveguides was achieved in Eagle2000. Optimal results can be obtained for very high scanning velocities of ≈10 cm/s, enabling the mass fabrication of devices employing such optical platforms. Exposing such waveguides to the surface is also possible while retaining their general spectral characteristics, opening a gateway to the production of optical sensors.

References

Amorim, V. A., J. M. Maia, D. Viveiros and P. V. S. Marques. 2019. "Loss Mechanisms of Optical Waveguides Inscribed in Fused Silica by Femtosecond Laser Direct Writing". *Journal of Lightwave Technology* 37 (10):2240-2245. DOI: 10.1109/JLT.2019.2900913.

Acknowledgments

This work was supported by Fundação para a Ciência e Tecnologia through grant no. SFRH/BD/128795/2017 and by Project "On Chip Whispering Gallery Mode Optical Microcavities For Emerging Microcontaminant Determination In Waters" - SAFE WATER, which is supported and co-funded by the European Commission, Directorate-General Communications Networks, Content and Technology (DG CONNECT) under the ERA-NET Cofund scheme - Horizon 2020 "Horizon 2020 – the Framework Programme for Research and Innovation (2014-2020)".

Fabrication of periodic structures in optical fibers by femtosecond laser micromachining

Duarte Viveiros[1,2], João M. Maia[1,2], Vítor A. Amorim[1,2], Pedro A. S. Jorge[1,2], P. V. S. Marques[1,2]

[1] Center for Applied Photonics, INESC TEC, Rua Dr. Roberto Frias, 4200-465 Porto, Portugal (carlos.d.viveiros@inesctec.pt), (joao.m.maia@inesctec.pt), (vitor.a.amorim@inesctec.pt)
[2] Department of Physics and Astronomy, Science Faculty, University of Porto, Rua do Campo Alegre, 4169-007 Porto, Portugal (pedro.jorge@fc.up.pt), (psmarque@fc.up.pt)

Abstract

A femtosecond laser direct writing system was developed (in order) to fabricate periodic structures in optical fibers. Writing of type I first- and second-order Bragg gratings (FBGs) in the same single-mode fiber (SMF-28e), with reflectivities of 99.6 % and 59.3 % respectively, is presented. The fabrication of long-period fiber gratings (LPFGs) in a SMF-28e fiber is also demonstrated. The LPFG presented in this work was fabricated with a period of 388 µm and a length of 60 mm.

Author Keywords. Femtosecond laser system, fiber Bragg gratings, long period fiber grating**.**

1. Introduction

Fiber gratings are employed as in-fiber optical filters and reflectors in telecommunication systems, fiber lasers, and sensors. Traditionally, they are fabricated by ultraviolet (UV) laser exposure through a periodic pattern created by two-beam interference (Haque et al. 2015). Their importance as devices for manipulating fiber guided light has led, in this work, to the development of a femtosecond laser direct writing system to explore the fabrication of periodic structures in optical fibers. The system has been primarily designed for the fabrication of point-by-point first order Bragg gratings, which is made possible due to the high spatial resolution ensuing from the non-linear absorption process triggered by fs-laser irradiation. However, this system has also been used to fabricate second order Bragg gratings and long period fiber gratings in a single-mode fiber (SMF-28e), showing its versatility. The spectral properties of each structure are presented.

2. Materials and Methods

A fiber amplified fs-laser (Satsuma HP, from Amplitude Systèmes), with a second harmonic beam at 515 nm and a pulse duration of approximately 250 fs at 500 kHz, was used to induce the periodic refractive index modification in the optical fiber's core. Before writing, the coating of the optical fiber was removed around the writing section, and the fiber was mounted on an XYZ stage. Two different lenses were used to focus the laser beam inside the fiber core to fabricate the FBGs and the LPFG: a 100× oil immersion lens (Olympus PLN 100XO), with a numerical aperture (NA) of 1.25, and a 40× aspherical lens (Newport 5722-A-H), with a NA of 0.55, respectively. During the fabrication of the structures, the laser gate was externally controlled by a periodic square time function with a duty cycle of 50 % generated by a synthesized function generator. This simple arrangement allows the automated writing of gratings with a given period by tuning the modulation frequency while translating the fiber at a given constant velocity.

Figure 1 (a) shows an example of a first- and second-order FBG whose properties have been summarized in Table 1. Figure 1 (b) displays the transmission spectra of a femto-inscribed LPFG with a period of 388 I.lm and a length of 60 mm.

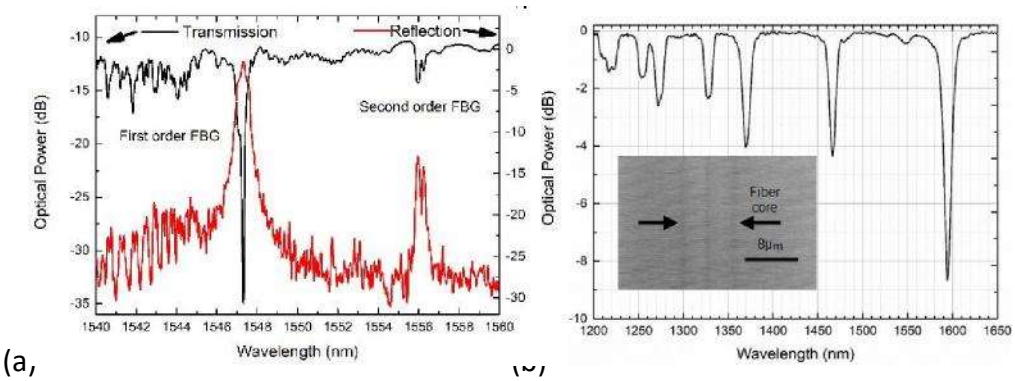

(a, (b)

Figure 1: Femtosecond laser spectrums of femto-inscribed: (a) FBGs and (b) LPFG (inset: grating structure inside the optical fiber core).

Fabrication Parameters					FWHM (nm)	Dip Attenuation (dB)	Reflectivity (%)
Grating order	Pulse Energy (nJ)	Scan velocity (μm/s)	Bragg Wavelength (nm)	Length (mm)			
First	63	50	1547.32	10	0.17	24.04	99.6
Second			1555.97		0.49	3.90	59.3

Table 1: Parameters of the femto-inscribed FBGs in an SMF-28e.

The optimum conditions to write LPFGs in SMF28e were attained with 130 nJ on-target pulse energy and 50 μm/s scan speed.

3. Conclusions

In this work, a femtosecond laser direct writing system was developed to explore the fabrication of periodic structures, namely FBGs and LPFG, in optical fibers. The possibility to write first- and second-order Bragg gratings in the same fiber was shown. The FBGs can be used for measuring and monitoring several parameters, such as strain, temperature, pressure, displacement, voltage, or electric current. The fabrication of LPFGs was also demonstrated, which opens the possibility to explore different types of sensors configurations like point (a single sensor location), distributed (continuous sensor) or quasi-distributed (multiple sensor locations) sensor. The LPFGs can be used to measure external perturbations, as mechanical stress, temperature, humidity, analyze chemical concentration or refractive index (RI) changes in the surrounding medium.

References

Haque, Moez, Jason R Grenier, Kenneth K C Lee, Luís a. Fernandes, and Peter R Herman. 2015. "Femtosecond Laser 3D Writing: From Smart Catheters to Distributed Lab-in-Fiber Sensing." *SPIE Newsroom*, 6–8. https://doi.org/10.1117/2.1201505.005979.

Acknowledgments

This activity is supported by a grant, SFRH/BD/110035/2015, from the Ministry of Education and Science of the Portuguese Government. The results presented in this paper are part of the Project "On Chip Whispering Gallery Mode Optical Microcavities For Emerging Microcontaminant Determination in Waters" – SAFE WATER, supported and co-founded by the European Commission, Directorate-General Communications Networks, Content and Technology (DG CONNECT) under the ERA-NET Cofund scheme – Horizon 2020 "Horizon 2020 – the Framework Programme for Research and Innovation (2014-2020)".

Laser induced breakdown system optimization and its applications

Miguel F.S. Ferreira[1,2], Diana Guimarães[2], Cátia Dias[3,4], Ricardo Ribeiro[3,4], Alexandre Lima[3,4], Rui C. Martins[2], Pedro A. S. Jorge[1,2]

[1] Department of Physics and Astronomy, Faculty of Sciences of the University of Porto, Rua do Campo Alegre, 4169-007, Porto, Portugal
[2] INESC TEC, Campus da FEUP, Rua Dr. Roberto Frias, 4200-465 Porto, Portugal
[3] Department of Geosciences, Environment and Spatial Plannings, Faculty of Sciences, University of Porto, Rua do Campo Alegre, 4169-007, Porto, Portugal
[4] Institute of Earth Sciences, Faculty of Sciences, University of Porto, Rua do Campo Alegre, Porto, Portugal

Abstract

A laser induced breakdown spectroscopy system was developed for field and laboratory operation. This system was improved with a sapphire window to protect the lens from material ejection and with three stages to allow for an easy sample positioning and mapping. A database composed of minerals was created to train the spectral recognition and quantification. System parameters, such as laser energy and focus position, were optimized in order to obtain better and more consistent results.

Author Keywords. Laser induced breakdown spectroscopy, Lithium, Mapping, Pattern recognition, Laser control

1. Introduction

Laser induced breakdown spectroscopy (LIBS) is a spectroscopy technique capable of analyzing samples in real time without the need of sample preparation (Musazzi and Perini 2014). This technique uses a pulsed laser to ablate, vaporize and ionize a small sample spot in order to form a plasma. After the plasma cooldown, the electrons start to recombine and the deexcitation of the elements results into the emission of photons with energies related to the difference between the energy levels of each element present (Cremers and Radziemski 2013). In this work, it is presented the development of a LIBS system and its applications for mining

2. Experimental Set-up

A LIBS set-up is composed of a laser focused through a lens onto the sample and a collection system that collects light emission through a fiber a redirecting it into a spectrometer. The system built uses a Nd:YAG laser (λ=1064 nm, 8 ns pulse length, M2=5.32 and 4.74 mm beam diameter) from Quantel and a 20 cm focusing lens. Eight fibers with collimators are used to collect the light to a high resolution eight channels spectrometer from AVANTES (16348 pixels, resolution 0.06-0.18 nm in the 180-926 nm range).

Material ejection occurs from the ablation of the sample. To protect the lens, a sapphire window with an anti-reflection coating was placed between the lens and the sample.

Three translational stages are used to allow a more precise sample 3D placement. With the help of two laser pointers, the precision of the sample localization in reference to the laser focus was greatly improved. The stages also improved the aiming and allowed the possibility of mapping samples (Figure 6).

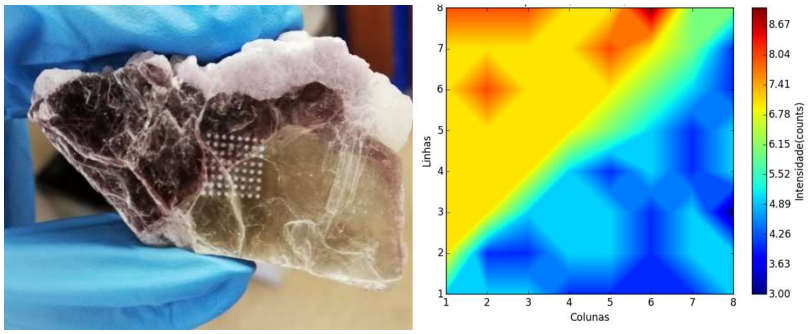

Figure 6: LIBS lithium mapping of a Lepidolite Li relative concentration in 70 x 70 mm map, in lepidolite and muscovite sample

3. Optimization and results

A database of several lithium (Li) and non-Li based minerals was used for training the spectral recognition and the quantification of Li content. This allowed for an easier identification of samples through pattern recognition.

The control of the pulse energy is also important. Different samples have different characteristics leading to different amounts of ablated and ionized material. By training the system with the optimized energies using PCA, the algorithm could adjust the energy by weighting the energies of the neighbors in feature space according to their distance to an initial low energy shot.

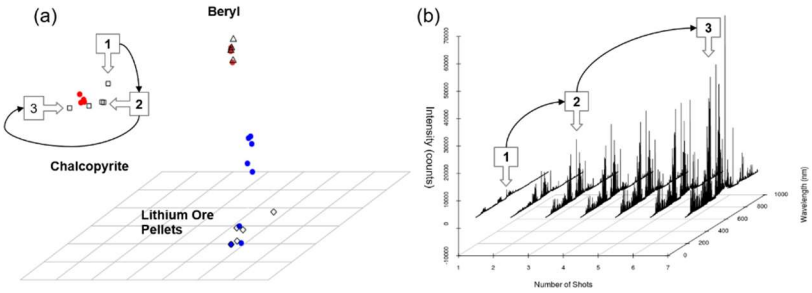

Figure 7: Increasing energy steps vs pattern recognition optimization: (a) projection in feature space of 10 fold increase in energy vs 3 pattern recognition optimization in chalcopyrite; and (b) corresponding spectra.

4. Conclusions

A LIBS system was built and it is capable of analyzing and mapping elements of complex samples using precision stages. Using PCA it is possible to find the most appropriate energy to analyze a sample in a small amount of iterations avoiding more damage to the surface.

References

Cremers, David A, and Leon J Radziemski. 2013. *Handbook of Laser-Induced Breakdown Spectroscopy Second Edition*. John Wiley & Sons Inc.

Musazzi, Sergio, and Umberto Perini, eds. 2014. *Laser-Induced Breakdown Spectroscopy*. Vol. 182. Springer Series in Optical Sciences. https://doi.org/10.1007/978-3-642-45085-3.

Acknowledgments

This work is funded by National Funds through FCT - Portuguese Foundation for Science and Technology within the scope of a PhD scholarship with the reference SFRH/BD/130680/2017 and the project under the reference PTDC/EEIEEE/31165/2017 and FEDER funds through the COMPETE 2020 Programme under the project number POCI-01-0145FEDER-031165.

Optical properties of a composite layer containing graphene and plasmonic particles.

Tiago Queirós[1,2], Mikhail Vasilevskiy[1,2], Pedro Alpuim[1,2]

[1] INL - International Iberian Nanotechnology Laboratory, Braga, Portugal.

[2] CFUM - Center of Physics of the University of Minho, Braga, Portugal.

Abstract

Graphene is a prime candidate for the development of metamaterials due to its unique properties. This work studies the special optical properties of a graphene and polarizable particles composite layer, which are prepared either using titanium microspheres, or SiO_2 disks lithographically patterned over graphene on Si substrates, and whose optical responses are measured using FTIR spectroscopy, and modulated by changing the graphene's Fermi level via chemical doping. Graphene based metamaterials show great promise for exploration and development of technology functioning at frequencies in the so called terahertz gap, which is still a comparatively underutilized range of the electromagnetic spectrum.

Author Keywords. Graphene, plasmonics, surface plasmon-polaritons, particle polarizability, metamaterials, terahertz radiation.

1. Introduction

Graphene can sustain surface plasmons. Distinctive features of graphene plasmonics are the strong response in the THz, a challenging, largely unexplored range of the electromagnetic spectrum due to the lack of natural materials that interact with THz radiation in a controlled manner, and tunability of surface plasmon-polaritons by manipulation of the Fermi level position. This project aims to show that the electromagnetic interaction of polarizable particles and graphene in a composite layer provides a mechanism for plasmon formation in the THz gap range.

2. Materials and Methods

A study of the effect of particle geometry on the optical response of the particle-graphene composite was conducted using Wolfram Mathematica. Graphene electrolyte-gated field-effect transistors were used to study the chemical doping resulting from the use of: 20% ethanol; 100mM ethanolamine; 50-60% hydrazine; and 7% 1-Pyrenebutyric acid N-hydroxysuccinimide ester (PBASE) in ethanol, by looking at the position of the charge neutrality point in a set of transistor transfer curves obtained after each of the doping steps. Optical lithography was used to form 10 I.lm in diameter and 2.5 I.lm tall SiO2 disks over high resistivity Si substrates, to mimic ellipsoid particles. Samples were prepared by manually transferring CVD grown graphene onto high resistivity Si substrates with and without disks. A coating of 47 I.lm diameter titanium microspheres and polyvinyl alcohol was applied to the substrates without disks. Optical measurements were collected using a Bruker IFS 66v FT IR spectrometer using 1 cm^{-1} resolution and a mercury lamp to generate FIR radiation.

3. Discussion

The simulation results of the system's optical response using different particle geometries are shown in Figure 1. Spheres resulted in a band pass-like transmittance spectrum and oblate particles lead to enhanced absorption, resulting in a dip in transmittance.

The chemical doping experiments indicate that 20% ethanol, 100mM ethanolamine and 50-60% hydrazine n-dope graphene, with hydrazine being the strongest. 7% PBASE in ethanol proved to dope p-type. The average position of the charge neutrality point (Dirac voltage) in

these samples is shown in Table 1. The averages refer to 17, 21, 4 and 14 measurements, respectively, and the errors are one standard deviation.

None of the expected features observed in the simulations were seen so far in the FT IR measurements. This might be due to the technical difficulty of assembling the composite layer. Raman analysis of the sample with the disks, made after FT IR, showed that the suspended graphene film ruptured upon insertion in the spectrometer vacuum chamber. On the other hand, the large size and weight of the Ti particles make it very difficult to produce and spread evenly a film of particles over graphene, with the desired concentration.

3.1. Figures

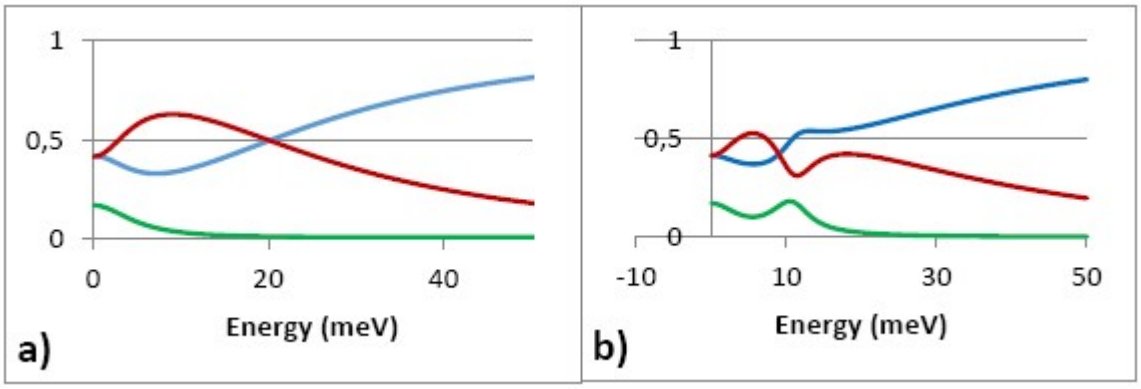

Figure 1: Calculated transmittance (Red), reflectance (Blue) and absorption (Green) spectra for the composite layer, considering the particles as: a) 47µm diameter Ti spheres with surface density of 2×10^{-4} µm^{-2} and b) Au oblate particles of radius 6.3µm and effective height to graphene of 3.15µm and surface density of 20×10^{-4} µm^{-2}. Parameters: Ef = 0.171eV, Γ= 3.7 meV, ε1 = 1 and ε2 = 10.68.

3.2. Tables

Doping agent	Dirac Voltage shift (V)
20% ethanol	-0.631 ± 0.077
100mM Ethanolamine	-0.241 ± 0.020
50-60% hydrazine	-0.757±0.0577
7% PBASE in ethanol	0.377±0.0761

Table 1: Average transistor Dirac voltage shift for different doping agents.

4. Conclusion

Graphene based composite layers might provide an easily tunable way to manipulate light in the FIR range and develop technology capable of interacting with light in the THz gap, however the means of assembling these layers must be further developed to confirm the phenomena uncovered by the simulations using these materials.

References

Souto, A., R.M.S. Pereira, J.E. Santos, N.M.R. Peres, M. Vasilevskiy, "Electromagnetic properties of a monolayer of polarisable particles deposited on graphene", V 10453, 3rd Int. Conf. on Appl. of Optics and Photonics, https://doi.org/10.1117/12.2271960 .

Acknowledgment

We thank A. Bondarchuk (INL) and L. Vieira (CFUM) for assistance with the FT IR measurements, and C.-D. Liao, J. Borme and S. Tkachev (INL) for help with sample preparation. This work was supported by the FCT in the framework of the Strategic Funding UID/FIS/04650/2013 and by FEDER project POCI-01-0145-FEDER-028114 (GRAPHSENS).

Vibration detection on power transformers using optical fiber sensors

Catarina S. Monteiro[1,2], António Vaz[2], Duarte Viveiros[2], Cassiano Linhares[4], S.M.O. Tavares[4], Hélder Mendes[4], Susana O. Silva[2,3], Paulo V. S. Marques[2,3], Orlando Frazão[2,3]

[1] Faculdade de Engenharia, Universidade do Porto, Rua Dr. Roberto Frias s/n, 4200-465 Porto, Portugal
[2] Instituto de Engenharia de Sistemas e Computadores, Tecnologia e Ciência, Rua Dr. Roberto Frias s/n, 4200-465 Porto, Portugal
[3] Faculdade de Ciências, Universidade do Porto, Rua do Campo Alegre 1021/1055, 4169-007 Porto, Portugal
[4] Efacec Energia, Máquinas e Equipamentos Eléctricos, S.A., Apartado 1018, 4466-952 S. Mamede de Infesta, Portugal

Abstract

Power transformers are an essential part of power transmission systems. Deterioration and aging of this systems can lead to sudden failure, causing damage of adjacent equipment or even service disruptions. Therefore, continuous monitoring of structural integrity is required. Optical fiber sensors can be used in the harsh environments provided by the power transformers. In this work, two vibration sensors composed by fiber Bragg gratings embedded in two different 3D printed cantilever structures were studied for vibration measurements.
Author Keywords. Fiber sensors, power transformers, fiber Bragg grating, vibration sensor

1. Introduction

Power transformers are static electric devices of uttermost importance. During operation, this devices can suffer from different stresses (Ma et al. 2015) that, together with aging, can cause system failure (Hashemnia, Abu-Siada, and Islam 2015). Power transformers health monitoring can be achieved by different methods (Deng et al. 2001), but conventional techniques fail to provide real time monitoring. Optical fiber sensors can overcome some problems. Embedding fiber sensors in different structures can lead to sensitivity enhancement. Structural analysis achieved by finite element analysis (FEM) together with 3D printing allows fast sensor prototyping. In this work, these tools were used for designing two different cantilever-based structures for vibration sensing using FBGs. The two structures were characterized for their vibration response for frequencies between 60 and 250 Hz.

2. Materials and Methods

The design of the sensors was done considering the maximum space available at the power transformer: 20 mm width, 65 mm length and 6 mm height. The two structures were designed to enhance deformation of the fiber due to the applied vibration and, to determine the region of maximum deformation, FEM analysis was performed. The FEM analysis considered the characteristics of the imprinting material: acrylonitrile butadiene styrene (ABS). This study, presented in **Figure 1**, enabled the attachment of the FBG in the maximum strain region using a standard cyanoacrylate adhesive.

3. Discussion

Vibration characterization was carried out using a shaker, and the optical signal was acquired using the interrogator BraggSCOPE FS26, from HBM FiberSensing, with a maximum frequency of acquisition of 10kHz. The fast Fourier transform (FFT) was calculated for each temporal signal, enabling to attain the most relevant frequencies of vibration of the sensors, as presented in **Table 1**. The two structures respond accordingly to the applied vibration frequency, with a maximum error of 5.4%.

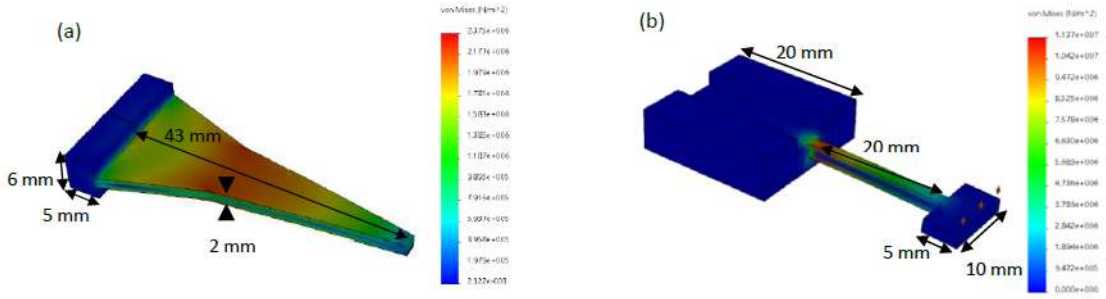

Figure 1: FEM analysis of (a) sensor 1 and (b) sensor 2.

Applied Frequency (Hz)	Sensor 1		Sensor 2	
	Readout Frequency (Hz)	Error (%)	Readout Frequency (Hz)	Error (%)
60	59.8	0.3	59.3	1.2
100	100.1	0.1	99.7	0.3
140	139.1	0.6	138.9	0.8
200	196.6	1.7	197.11	1.4
250	245.3	1.9	236.6	5.4

Table 1: Experimental results for the main vibration frequencies in respect to the applied frequency, for the two structures

4. Conclusions

In this work, two cantilever-based sensing structures were studied for vibration detection using FBGs. The mechanical behavior of two structures to a 1-dimensional displacement was studied using FEM analysis. The two FBGs were attached to each 3D printed structure, that allowed an easy and fast prototyping. The sensors were subjected to uniaxial excitation frequencies up to 250 Hz, achieving a maximum error of 5.4%.

References

Deng, Jiangdong, Hai Xiao, Wei Huo, Ming Luo, Russ May, Anbo Wang, and Yilu Liu. 2001. "Optical Fiber Sensor-Based Detection of Partial Discharges in Power Transformers." *Optics and Laser Technology* 33 (5): 305–11. https://doi.org/10.1016/S0030-3992(01)00022-6.

Hashemnia, Naser, A. Abu-Siada, and S. Islam. 2015. "Improved Power Transformer Winding Fault Detection Using FRA Diagnostics – Part 1: Axial Displacement Simulation." *IEEE Transactions on Dielectrics and Electrical Insulation* 22 (1): 556–63. https://doi.org/10.1109/tdei.2014.004591.

Ma, Hui, Tapan K. Saha, Chandima Ekanayake, and Daniel Martin. 2015. "Smart Transformer for Smart Grid - Intelligent Framework and Techniques for Power Transformer Asset Management." *IEEE Transactions on Smart Grid* 6 (2): 1026–34. https://doi.org/10.1109/TSG.2014.2384501.

Acknowledgments

C.S. Monteiro was financed by FCT - Portuguese national funding agency for science, research and technology (SFRH/BD/135820/2018). This work is supported by the project POCI-01-0247-FEDER-024035, with the acronym Quiet Transformer 2, co-funded by the European Regional Development Fund (ERDF) through COMPETE2020 - Programa Operacional de Competitividade e Internacionalização (POCI) under the "Portugal 2020" Programme.

Fibre-integrated phase-change devices

Tiago Martins[1,2], Behrad Gholipour2, [3], Davide Piccinotti[2], Jun-Yu Ou[2], Kevin F. MacDonald[2], Orlando Frazão[1], Anna Peacock[2] and Nikolay I. Zheludev[2,4]

[1] INESC TEC and Department of Physics and Astronomy, Faculty of Sciences, University of Porto, Rua do Campo Alegre, 687, 4150-179 Porto, Portugal

[2] Optoelectronics Research Centre and Centre for Photonic Metamaterials, University of Southampton, Southampton, SO15 4JB, UK

[3] Department of Chemistry, University of Southampton, Southampton, SO15 4JB, UK

[4] Centre for Disruptive Photonic Technologies & The Photonics Institute, School of Physical and Mathematical Sciences, Nanyang Technological University, 637371, Singapore

In order to realize the goal of bringing together chalcogenide material functionality and optical fibre platforms, two device configurations are proposed, one based on combining a thick GST film with a side-polished fibre and the other relying on a periodically structured film of the same phase-change material deposited on the flat facet of a cleaved fibre tip. In both designs, the chalcogenide film is placed within close proximity to the region of the waveguide where light is guided through, either promoting interaction of an evanescent nature, as is the case of the side-polished-based architecture, or leading to a scenario characterized by stronger light-matter interplay, as is the case of the fibre-tip device in which the GST layer intercepts light propagation through the fibre core. Under both these circumstances, induced structural phase changes of the chalcogenide material, inevitably linked to pronounced variations of its optical parameters, are expected to pave the way for considerable light modulation ratios, with potential applications in non-volatile memory devices, with the added advantage of possible integration with widespread and extensively used waveguiding structures.

Fabrication of RFID antennas in thin membranes of Parylene-C for wearable applications

Leonor Duarte[1,2], Joana P. Neto[1] and Joana Vaz Pinto[1]

[1] i3N/CENIMAT, DCM, Faculdade de Ciências e Tecnologias, Universidade Nova de Lisboa, Campus de Caparica, 2829-516 Caparica, Portugal

[2] Departament of Physics, Faculdade de Ciências e Tecnologias, Universidade Nova de Lisboa, Campus de Caparica, 2829-516 Caparica, Portugal

Abstract

Wearable devices for continuous monitoring of physiological health are a growing demand in our days. These devices must be thin, flexible, small and, at the same time, durable and capable of precise measurements. In addition, besides being wearable, these electronic devices should be wireless to allow the communication with smartphones and other devices [1]. As a response to the need of flexible and conformable sensors, we propose the use of Parylene-C membranes as substrate since, with this polymer, it is possible to produce ultra-thin membranes (1 µm to 5 µm thickness) that are biocompatible, transparent, flexible and able to mimic human skin [2, 3]. Previously, in CENIMAT, we proved that parylene has excellent properties as a substrate, insulator and encapsulation layer, by producing TFTs and capacitors, as well as UV sensors [3, 4, 5]. On the other hand, in order to ensure wireless and easy communication, we intend to fabricate in parylene a passive RF antenna that, combined with an IC chip, will make a RFID tag that works at 13.56 MHz and may communicate with the developed devices and sensors. A passive tag it's a simple and cheaper system, compared with an active, since it has no power source [6], and uses power emitted from a reader, based on an inductive coupling [7]. Therefore, in these systems a matching between the antenna and chip impedances (Z) must be insured [8].

Author keywords: Parylene-C, RF antenna, RFID system, Wearable devices, Impedance Spectroscopy.

In this project we produced thin film antennas using different metals like copper, aluminium, chromium, titanium and gold, deposited by PVD techniques (e.g., thermal and e-beam evaporation, RF magnetron sputtering). Different antennas were tested, considering different parameters like its resistance (R) and inductance (L) that affect the resonance frequency () of tag [9], as well as the internal chip capacitance (C), as given by equation 1:

$$f_{resonance} = \frac{1}{2\pi\sqrt{L\times C}} \qquad (1)$$

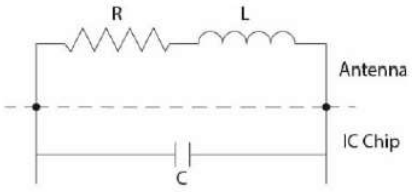

Figure 1 - Tag circuit diagram, consisting on a RF antenna and IC chip.

The inductance depends on the geometrical factors such as the number of coils (N), the width of the coils (w) and the spacing between coils (h) as expressed in equation 2, for a rectangular antenna [9]:

$$L = \frac{N^2\mu_0}{\pi}\left[-2(w+h) + 2\sqrt{h^2+w^2} - h\ln\left(\frac{h+\sqrt{h^2+w^2}}{w}\right) - w\ln\left(\frac{w+\sqrt{h^2+w^2}}{h}\right) + h\ln\left(\frac{2h}{a}\right) + w\ln\left(\frac{2w}{a}\right)\right] \quad (2)$$

Impedance spectroscopy was used to characterize the produced antennas, which allowed us to conclude that copper antennas have the best electrical response (Z, L), performing as a resistor-inductor circuit.

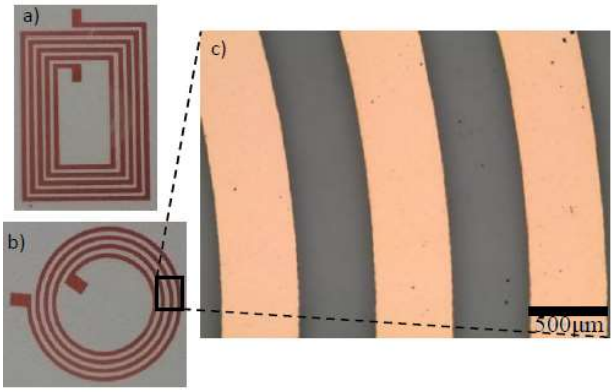

Figure 2 - Produced antennas made of copper. a) Rectangular (13,25 mm x 18,9 mm); b) Circular (18 mm x 18,5 mm); c) Optical microscope image of the circular antenna.

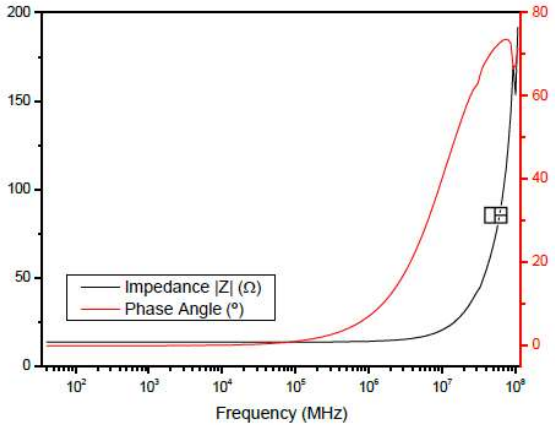

Figure 3 - Dependence of the impedance and phase angle as a function of the frequency.

In this project, the aim is to connect RFID antennas to specific developed sensors and devices fabricated in Parylene-C, with the purpose of reading and transmitting the signals detected with the formerly mentioned accomplished sensors. Since our system is based on NFC, we pretend to couple it with a RFID module and Arduino, that will serve as a reader, so we can control and communicate with the tag and consequently with the sensor.

Ultimately, the final goal is to implement wireless, battery-free communication RFID system in wearable devices, that activates itself in the presence of a smartphone (reader) and can be used on the skin to monitor one parameter (e.g., pressure, temperature and UV intensity).

References

[1] J. Heikenfeld, J. Rogers, T. Pan, M. Khine, and J. Wang, "Lab on a Chip," vol. 18, no. 2, 2018.

[2] Y. Liu, "Novel Parylene Filter s for Biomedical Applications," Requirements for the degree of Doctor. California Institute of Techonology, 2016.

[3] M. Rolho, "Otimização de filmes de Parileno como Dielétrico para TFTs," Requirements for the degree of master. Faculdade de Ciências e Tecnologia, Universidade Nova de Lisboa, 2015.

[4] I. de O. Martins, "Parylene C as substrate , dielectric and encapsulation for flexible electronics applications," Requirements for the degree of master. Faculdade de Ciências e Tecnologia, Universidade Nova de Lisboa, 2017.

[5] V. C. Caniça, "Development of sensors in ultrathin membranes of Parylene C," Requirements for the degree of master. Faculdade de Ciências e Tecnologia, Universidade Nova de Lisboa, 2018.

[6] J. Zhang, G. Tian, A. Marindra, A. Sunny, and A. Zhao, "A Review of Passive RFID Tag Antenna-Based Monitoring Applications," *Sensors*, vol. 17, pp. 1–34, 2017.

[7] G. T. Resort, P. V Nikitin, K. V. S. Rao, S. Member, S. Lazar, and A. A. F. Regions, "An Overview of Near Field UHF RFID," in *2007 IEEE International Conference on RFID*, 2007, pp. 167–174.

[8] S. Kalayci, "Design of a Radio Frequency Identification (RFID) Antenna," Requirements for the degree of master. Middle East Technical University, 2009.

[9] "Application Note for MLX90129 - Antenna Design | Melexis." [Online]. Available: https://www.melexis.com/en/documents/documentation/application-notes/application-note-mlx90129-antenna-design. [Accessed: 28-Feb-2019].

Graphene Radio-Frequency Transistors with Self-Aligned Channel and Core-Shell Nanowire Gate

Lucas Baptista[1,2], Vitor Silva[1,2], Ivo Colmiais[1,2], Nan Zhang[1], Jerome Borme[1], Chun-Da Liao[1], Lifeng Liu[1], Paulo Mendes[2], Pedro Alpuim[1,2]

[1] International Iberian Nanotechnology, Avda. Mestre José Veiga, 4715-330, Braga, Portugal

[2] CMEMS, Universidade do Minho, Campus de Azurém, 4800-058, Guimarães, Portugal

Abstract

Graphene is considered an attractive material for future electronics, however the fabrication of devices is challenging as most of the CMOS technologies would damage graphene. In this work, nickel/nickel oxide core-shell nanowires, electrochemically grown using an AAO template, were used to work as gate and gate oxide, respectively, of an RF transistor and placed on the graphene channel. A self-aligned process is used to create source and drain contacts, perfectly aligned with the gate, thus reducing the access resistance in the ON state of the device. The device was designed and simulated to a cut-off frequency of 15 GHz.

Author Keywords. graphene RF transistors, cut-off frequency, core-shell nanowire, self-aligned channel.

1. Introduction

Graphene, a two dimensional material, has attracted great attention for the electronics of the future due to its amazing properties, which could enable RF circuits to function in the Terahertz regime (Liao and Duan 2012). However, standard CMOS dielectric integration processes introduce substantial defects into the graphene lattice, reducing the mobility of the charge carriers and in turn lowering the performance of the device. High access resistance due to incorrect alignment of the source-drain contacts has proven to be another fabrication issue regarding such devices. In this work, a RF-GFET fabrication process is proposed that uses a nickel/nickel oxide core-shell nanowire (NW) functioning as gate and gate dielectric, respectively, positioned on the graphene channel by electrophoretic means, thus minimizing defects introduced during fabrication steps and allowing for a source-drain self-aligned process, minimizing the access resistance.

2. Materials and Methods

Ni/NiO nanowire synthesis and handling. The Nickel nanowires were electrochemically grown using an Anodized Aluminum Oxide (AAO) template with a sputter deposited Au seed layer and a mixture of $NiSO_4$, $NiCl_2$ and H_3BO_3 using the setup shown in Figure 1a. The AAO template, previously bought from Smartmembranes, had porous diameters ranging from 200 to 400 nanometers and, after growth, the template was dissolved using a solution of NaOH 1M (Figure 1b). The nanowires were then thermally oxidized in an oven at 250 °C for 1 hour, resulting in a 5 nanometers thick shell of NiO surrounding the wire. The nanowires were released from the seed layer with a solution of Potassium Iodide (KI) and Iodine (I_2) and stored in an ethanol-based solution.

Device fabrication process. Highly resistive silicon substrates (>10kΩ.cm) with a 1-micron thick layer of silicon dioxide (SiO_2) were used to fabricate the devices. Graphene was grown by CVD on a copper foil and transferred onto the insulating substrate through a standard PMMA transfer. Ni/NiO nanowires were randomly deposited on top of the graphene film (Figure 1c) and with the aid of high resolution images of the surface and of TiW reference marks previously patterned by lift off, masks for the lithography steps were designed around the positions of the NWs (Figure 1d). Excess graphene was removed by oxygen plasma etching (Figure 1e) and a deposition of Cr/Pd (3 nm/30 nm), followed by

an ion milling process, defined the self-aligned contacts and pad connections to the device, fixing the channel width of 3 µm.

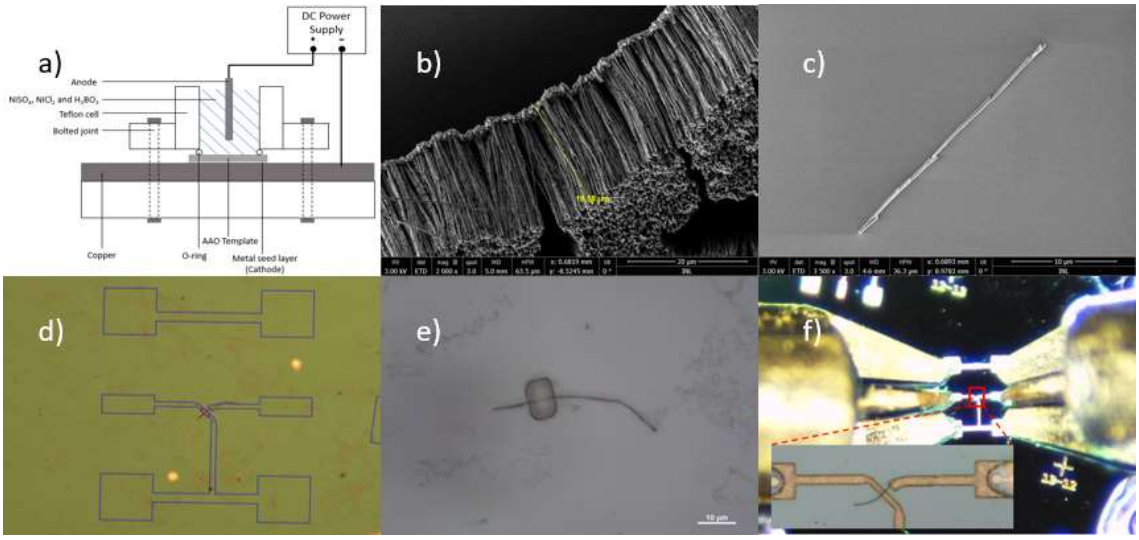

Figure 8: Fabrication steps for the RF-GFETs. a) Electrochemical deposition set up. b) Grown nanowires attached to the seed layer. c) SEM image of a single nanowire. d) AutoCAD masks for the devices. e) Lithography of the graphene channel. f) Contact between the RF probes and the pads of the RF device. Inset showing a close view of the core-shell Ni/NiO nanowire and the self-aligned Drain-Source contacts.

3. Discussion

Prior to its fabrication, the device was modelled using equivalent circuit components and a GFET current and transconductance model, projecting an estimated cut-off frequency of 15 GHz. However, the measured S-parameters showed that S12 and S21 were equal, indicating a clear mal-function of the device (Figure 1f). Upon further investigation, a resistance of 2.3 kΩ was measured from drain to gate indicating a short-circuit between these two contacts. This short is due to the wire covering the graphene during the channel lithography step, making it impossible for the oxygen plasma to access the entire region underneath it to remove the graphene until the edge of the channel.

4. Conclusion

In this work an RF GFET was modeled, fabricated and characterized. Because the fabrication process fell short of fully succeeding, a dielectrophoretic process is being developed to precisely place the nanowires on top of the already patterned graphene channel, guaranteeing that there is no short-circuit between the gate contact and the channel.

References

Liao, Lei, and Xiangfeng Duan. 2012. “Graphene for Radio Frequency Electronics.” *Materials Today 15 (7–8) 2012, 328-338*. https://doi.org/10.1016/S1369-7021(12)70138-4.

Acknowledgment

Supported by FCT funds: PTDC/EEI-TEL/29670/2017 - (POCI-01-0145-FEDER-029670), co-financed by the European Regional Development Fund (ERDF), and through COMPETE 2020.

Development of a Dual-Polarity Ion Drift Chamber

D.J.G. Marques[1,2], M.A.G Santos[4], A.F.V. Cortez[2,3], J. Escada[1,2], F.P. Santos[1,2] , A.M.F.Trindade[1,2], and F.I.G.M. Borges[1,2]

[1] Laboratory of Instrumentation and Experimental Particle Physics – LIP, Rua Larga, 3004-516 Coimbra, Portugal

[2]Department of Physics, Faculty of Science and Technology, University of Coimbra, Rua Larga, 3004-516 Coimbra, Portugal

[3] Laboratory of Instrumentation, Biomedical Eng. and Radiation Physics – LIBPhys, Rua Larga, 3004-516 Coimbra, Portugal

[4] Deimos Engenharia, SA, Nº 41, 10, Avenida Dom João II, 1998-023 Lisboa, Portugal

Abstract

In this paper, the working principle of a Dual-Polarity Ion Drift Chamber is explained, together with the first ion mobility experimental measurements made with it. We also present the problems that arose during its development and the future work that will be done in order to improve its performance, namely its accuracy and resolution.

Author Keywords. Gaseous detectors, Negative Ion Time Projection Chambers, Ion Drift Chamber, Ionization and excitation processes, Ion sources, Charge transport and multiplication in gas, Electron attachment.

1. Introduction

Ion mobility in a gaseous medium, K, is defined as the ratio between the particle drift velocity, v_d, and the applied electric field, E (Formula 1):

$$K = \frac{v_d}{E} \qquad (1)$$

This parameter is very important in the signal formation in gaseous detectors, since the ion cloud can affect the detector's response [1], especially in large volume detectors. Although in the most common detectors the ion's charge is positive, in Negative Ion Time Projection Chambers (NITPC), the negative ions are responsible for the signal formation, and the information about their mobility in the parent gas is an essential parameter for the gas choice in these chambers [2].

1.1. Methodology

The ion's velocity is obtained by measuring the time that the ions take to drift under a uniform electric field, from a GEM where they are originated to a collecting grid located above it.

To create such ions, a UV flash lamp hits a CsI photocathode deposited on top of the GEM surface, originating photoelectrons that are guided to the GEM's holes, where they ionize or attach to the gas molecules, originating either positive or negative ions. After leaving the GEM's holes, these ions drift under a uniform electric field, towards a double-grid (Frisch grid and collecting grid), where they are collected, originating a time spectrum of the ions' arrival time. With these values, the drift velocity and ion mobility can be obtained.

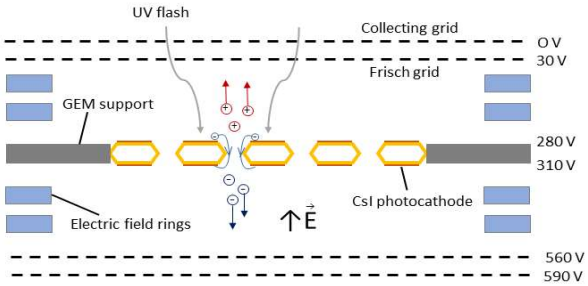

Figure 9: Experimental system schematic

2. First prototype

2.1. Design

The drift chamber schematic is shown in figure 1, together with the processes that occur inside it. Having the GEM in the middle of the chamber and field rings on both sides, it is possible to create different electric fields allowing for the study of both negative and positive ions, either separately or at the same time. It is important to note that the real system has 4 field rings in each side.

2.2. Limitations

1) The trigger peak from the light source was found to be 200 times greater than expected.
2) The electric field inside the chamber was proven to be not uniform, being much stronger next to the GEM and the field rings.
3) The overall system noise was much higher than expected and the test results with Ne and CF_3 showed to have low accuracy and a low peak resolution.

The main reasons for these limitations are believed to be due to the non-uniformities in the electric field.

2.3. GEM base new design

The new GEM base design (under construction) consists in placing the GEM between two stainless steel discs which are separated by a kapton foil (containing the GEM) and make electric contact with the it (figure 2). With this, is it possible to bias the GEM by providing different voltages to the discs and, which is the main objective, to reduce almost entirely the electric field non-uniformities.

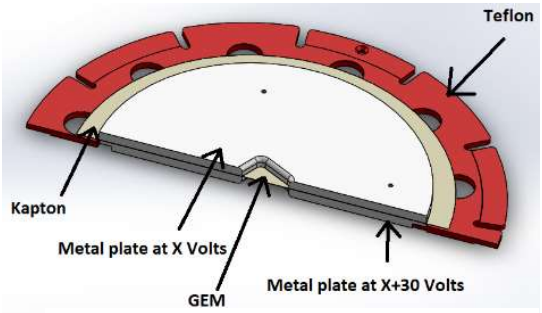

Figure 10: New GEM base design

3. Expectations

With the previously described change, we expect to lower the noise background and improve both resolution and accuracy of the chamber. The expected electric field inside the chamber has already be simulated (figure 3).

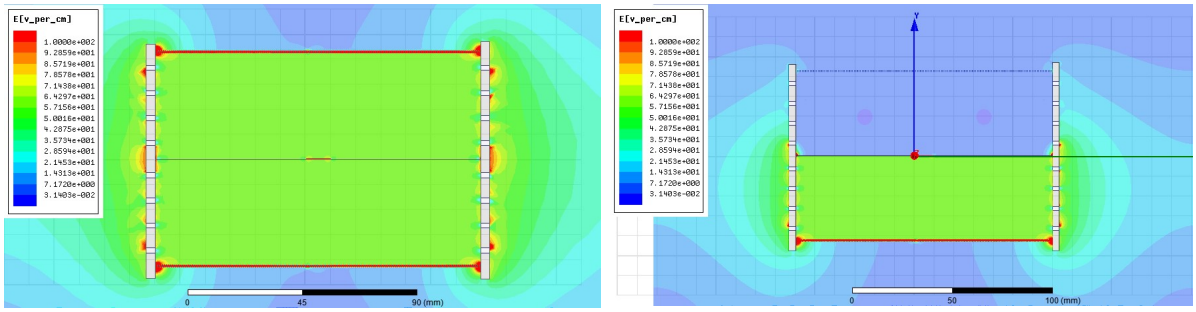

Figure 3: Expected electric field inside the chamber with (left) both sides biased acquiring signals from both positive and negative ions; (right) only one side biased and the other at same voltage as the GEM.

References

[1] Knoll, Glenn F. 1979. Radiation detection and measurement. New York: Wiley.

[2] Martoff, D. Snowden-Ifft, T. Ohnuki, N. Spooner, and M. Lehner. Suppressing drift chamber diffusion without magnetic field. Nucl. Inst. and Meth. Phys. A., 440(2):355 – 359, 2000. ISSN 0168-9002

Acknowledgments

David J. G. Marques acknowledges a Scientific Initiation Scholarship, through project "Participation in the RD51 Collaboration" (CERN/FIS/INS/0025/2017).

A One-Pot Synthesis Method of Chitosan Magnetic Composite Structures for Sensing in Biomedicine

Francisca Gomes[1], Inês Cruz[1], Mariana Rocha[2], Paula Parreira[3], Cristina Martins[3], Clara Pereira[2], and André M. Pereira[1]

[1] IFIMUP-IN, Department of Physics and Astronomy, Faculty of Sciences, University of Porto, Rua do Campo Alegre s/n, 4169-007, Porto, Portugal

[2] REQUIMTE/LAQV, Department of Chemistry and Biochemistry, Faculty of Sciences, University of Porto, Rua do Campo Alegre s/n, 4169-007, Porto, Portugal

[3] i3S—Instituto de Investigação e Inovação em Saúde, University of Porto, Rua Alfredo Allen 208, 4200-135, Porto, Portugal

Abstract

Magnetic nanocomposites have an extraordinary potential in numerous areas of Science and Medicine due to their outstanding physical and chemical behavior. Biomedical research has particularly focused on the combination of such materials with biocompatible polymers for a myriad of purposes, ranging from antimicrobial treatment to biosensing and theranostics. Metal oxide magnetic nanoparticles (MNPs) are one such example, having already been coated with silica, alginate, chitosan, polycaprolactone, poly(lactic-co-glycolic acid), among other shells. Typically, the preparation of these multifunctional nanomaterials is a two-step procedure involving the synthesis of the MNPs, followed by a chitosan coating through chemical methods. However, and most importantly, works describing the one-pot preparation of these multifunctional biomaterials are still scarce. We hereby present a simple and innovative protocol for the one-pot synthesis of chitosan-coated superparamagnetic nanoparticles, leading to the production of chitosan-coated magnetite (Fe_3O_4@Chi) and chitosan-coated manganese(II) ferrite ($MnFe_2O_4$@Chi) as Hall effect biomarkers for medical diagnostics.

Author Keywords: *Superparamagnetic nanoparticles, chitosan, biosensors, biomarkers*

1. Introduction

Planar Hall effect sensors have been indicated as a promising detection method of magnetic nanoparticles (MNPs) in various applications, particularly in biosensing. Surface functionalization with appropriate molecules ultimately confers exceptional biomarker properties. Spinel ferrites (MFe_2O_4, where M(II) = Co, Fe, Mn, etc.) are cubic crystal structures with extraordinary magnetic properties, namely superparamagnetism at nanometer sizes and very low coercivity fields (Pereira et al. 2012). Examples such as magnetite (Fe_3O_4) or manganese(II) ferrite ($MnFe_2O_4$) evince high saturation magnetization (M_s) and no remanent magnetization, being ideal for biomedicine. Notwithstanding their potential, these materials have shown slight cytotoxicity and bioaccumulation (Zhao et al. 2015). To overcome this drawback, one solution is their coating with biocompatible shells. Chitosan is a biocompatible and biodegradable natural polymer derived from chitin (Fernandes et al. 2013), and so the combination of ferrite with chitosan has been deemed as a promising solution. Typically, the preparation of these multifunctional materials is a two-step process involving the synthesis of the MNPs followed by a chemically assisted chitosan coating. However, works describing a one-pot preparation of these composites are still scarce.

The purpose of this work is to simplify the currently published core-shell chitosan-ferrite production protocols by conjugating chitosan purification with ferrite coprecipitation synthesis in a one-pot process. This is the first step in the production of Hall effect biomarkers for biosensing.

2. Discussion

The characterization of Fe_3O_4@Chi and $MnFe_2O_4$@Chi was made through dynamic light scattering (DLS), X-ray diffraction (XRD), scanning electron microscopy (SEM), energy dispersive spectroscopy (EDS), Fourier transform infrared spectroscopy (FT-IR), Raman spectroscopy and SQUID magnetometry. The results proved the presence of both chitosan and magnetic nanoparticles in the samples (**Figure 2**), with unchanged superparamagnetic regime of the bare MNPs.

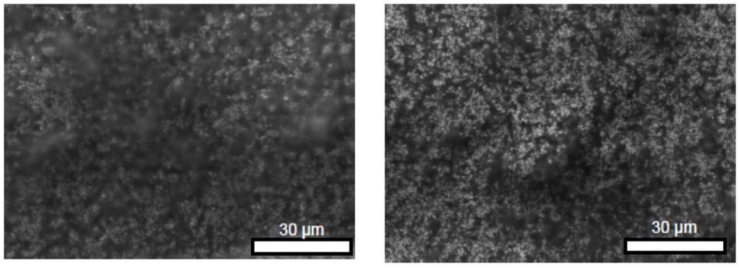

Figure 11 SEM images of Chi@Fe3O4 (left) and Chi@MnFe2O4 (right).

3. Conclusions

Superparamagnetic NPs with high M_S (Fe_3O_4: 41 emu g^{-1}; $MnFe_2O_4$: 65 emu g^{-1}) were coated with chitosan through a one-pot method, and preliminary crosslinking results showed the formation of micrometric structures of chitosan-coated MNPs. Future work will focus on further magnetization studies and crosslinking optimization for the production of magnetic chitosan with high performance in biosensing applications.

References

Fernandes, M., I. C. Goncalves, S. Nardecchia, I. F. Amaral, M. A. Barbosa, and M. C. Martins. 2013. "Modulation of stability and mucoadhesive properties of chitosan microspheres for therapeutic gastric application." *Int J Pharm* 454 (1):116-24. doi: 10.1016/j.ijpharm.2013.06.068.

Pereira, Clara, André M. Pereira, Carlos Fernandes, Mariana Rocha, Ricardo Mendes, María Paz Fernández-García, Alexandra Guedes, Pedro B. Tavares, Jean-Marc Grenèche, João P. Araújo, and Cristina Freire. 2012. "Superparamagnetic MFe2O4 (M = Fe, Co, Mn) Nanoparticles: Tuning the Particle Size and Magnetic Properties through a Novel One-Step Coprecipitation Route." *Chemistry of Materials* 24 (8):1496-1504. doi: 10.1021/cm300301c.

Zhao, Hongli, Zongyan Chen, Liang Tao, Xiang Zhu, Minbo Lan, and Zhen Li. 2015. "In vitro toxicity evaluation of ultra-small MFe2O4 (M = Fe, Mn, Co) nanoparticles using A549 cells." *RSC Advances* 5 (84):68454-68460. doi: 10.1039/C5RA11013K.

Acknowledgments

The authors acknowledge funding from Fundação para a Ciência e a Tecnologia (FCT) and COMPETE 2020 in the FEDER component, Project NECL - NORTE-01-0145-FEDER-022096, Project UID/NAN/50024/2019 and Project PTDC/CTM-BIO/4043/2014. C.P. thanks FCT for the FCT Investigator contract IF/01080/2015.

Image Processing and Object Detection for Advanced Driver-Assistance Systems

André Gabriel[1,2], João Silva[2], Isabel Catarino[1]

[1] LibPhys-UNL, DF, Faculdade de Ciências e Tecnologias, Universidade Nova de Lisboa, Campusde Caparica, 2829-516 Caparica, Portugal
[2] ALTRAN PORTUGAL - R&D, Av. D. João II, Lote 1.07.2.1 Piso 2, 1990-096, Lisboa, Portugal

Author Keywords. Autonomous Driving; ADAS; Stereo Vision System; LiDAR; Deep Learning; ROS.

Every year thousands of deaths are caused by car accidents all over the world. Human errors are considered the major responsible since people are becoming increasingly sloppy [1]. To preclude this problem and improve the safety on public roads as well as quality of human life, the concept of Autonomous Driving was introduced. It consists on the implementation of a system in a car that is specially designed to drive without human intervention. However, a fully autonomous system that operates without failures has still not been conceived.

This work aims to contribute to the progress in the area of Autonomous Driving by developing a software to identify the environment around a vehicle. This software is implemented with Robot Operating System (ROS) framework [2] and it has three main objectives: the application of deep learning for object detection, depth estimation with image processing and LiDAR data analysis modules. The ROS framework provides several tools that helps building a complex software in a simpler way. It also allows to create a solid and effective infrastructure to build the code on, with a good communication between different tasks. Moreover, it was used real-life situations from KITTI dataset [3] to test and develop the software.

An existing deep learning module has been used to perform object detection. The model was provided by the official Tensorflow GitHub website [4] and it was trained with COCO dataset [5], comprising 90 different classes. It was also designed with a Single Shot Detector (SSD) [6] and MobileNet [7] architectures. The SSD allows the object localization and classification in a single forward pass of the network while the MobileNet composes lighter deep learning networks build from depthwise separable convolutions.

The trained model only performs on the left images of the stereo vision system (Figure 1 (a)). On the right images, it is applied a template-matching algorithm from Python OpenCV library [8]. It extracts every detection on the left image and finds its match on the right image, as showed on Figure 1 (b). This methodology saves computational power and, consequently, saves performing time. It uses six methods to find the best match: square difference, cross-correlation, correlation coefficient and the same three normalized [9]. Due to small deviations on each match position, the matching bounding boxes are slightly increased, compared to the model bounding boxes, ensuring that the object is absolutely inside it.

Regarding the depth perception module, both bounding boxes of the same object (left and right) are extracted to be analyzed by the SIFT feature detector and matcher [10]. This algorithm is also provided by the Python OpenCV library and it does not only search for features on both images but also matches them. To improve the match accuracy, two filters were developed: one to filter the matching process and other to filter the matched features that went through the previous step. The filter used on the matching phase ensures that the features that get matched are in similar regions. The matched features filter is used to

exclude matches if their disparity diverges from the majority disparity agglomeration. Considering the best matches, an average disparity is calculated to find the depth of the object. As cameras are calibrated with the same height and they provide images within the same plane, the following equation is used to depth estimation.

$$depth = \frac{baseline * focal\ length}{disparity}, \quad \text{where:} \quad disparity = x_{left} - x_{right}$$

Figure 1 (a) Left image. Model performance; (b) Right image. Template-matching.

The last objective to integrate is the LiDAR data analysis module. It uses the Point Cloud Library (PCL) [11], which is integrated in the ROS framework, providing useful tools to understand and manipulate LiDAR point cloud data. There is an average of 120000 points on each point cloud frame that need to be processed and analyzed. First, to decrease the computational power needed, the number of points on each frame is decreased by a factor of two, without losing crucial information. On a second stage, the points that corresponds to the ground are removed. To do so, it is used a planar model to segment points that fits in a plane and removes them from the cloud. Then, a clustering model is used to agglomerate parts of the cloud of possible objects. With these clusters and their spatial positioning, the distance between them and the car is calculated.

This communication discusses the progresses on the developed ADAS software along with the open issues to address in further work. The template-matching algorithm deviations sometimes are not close to what was supposed to match, due to the small size of bounding boxes. The SIFT algorithm has difficulties on detecting features on objects that were detected far away from the car. In addition, one of the next steps on this project is to create a data fusion module to merge all the information available from the different modules.

References

[1] T. Vanderbilt. “Traffic: Why we drive the way we do (and what it says about us).” In: *Information Design Journal* 17.2 (2009), pp. 152-152. DOI: 10.1075/idj.17.2.11foe.

[2] ROS. *Robot Operating System*. 2019. URL: https://www.ros.org (visited on 05/27/2019).

[3] A. Geiger, P. Lenz, C. Stiller, and R. Urtasun. “Vision meets robotics: The KITTI dataset.” In: *International Journal of robotics Research* 32.11 (2013), pp. 1231-1237. DOI: 10.1177/0278364913491297.

[4] Tensorflow GitHub. *Tensorflow detection model zoo*. 2019. URL: https://github.com/tensorflow/models/blob/master/research/object_detection/g3doc/detection_model_zoo.md (visited on 05/27/2019).

[5] T. Lin et al. “Microsoft COCO: Common Objects in Context.” In: *CoRR* (2014). arXiv: abs/1405.0312.

[6] W. Liu, D. Anguelov, D. Erhan, C. Szegedy, S. Reed, C. Fu and A. Berg, “SSD: Single Shot MultiBox Detector.” In: *CoRR* (2016). DOI: 10.1007/978-3-319-46448-0_2.

[7] A. Howard et al. “MobileNets: Efficient Convolutional Neural Networks for Mobile Vision Applications”. In: *CoRR* (2017). arXiv: 1704.04861.

[8] OpenCV. *AI Courses by OpenCV.* 2019. URL: https://opencv.org (visited on 05/27/2019).

[9] D. Stoitchkov. “Analysis of Methods for Automated Symbol Recognition in Technical Drawings”, Technical University of Munich, 2018.

[10] D. Lowe. “Distinctive Image features from Scale-Invariant Keypoints”. In: *“International Journal of Computer Vision”* 60.2 (2004), pp. 91-110. DOI: 10.1023/B:VISI.0000029664.99615.94.

[11] PCL. *Point Cloud Library.* 2019. URL: http://pointclouds.org (visited on 05/27/2019).

POSTERS

The Topological Surface State on a Variable Range Hopping dominated conduction Sb2Te3 sputtered thin film

Sofia Ferreira-Teixeira[1,2], Ana L. Pires[1], Will R. Branford[2], João P. Araújo[1], Lesley F. Cohen[2], André M. Pereira[1]

[1] IFIMUP, Institute of Physics for Advanced Materials, Nanotechnology and Photonics, University of Porto, Rua do Campo Alegre, 687, 4169-007, Portugal

[2] Physics Department, Blackett Laboratory, Imperial College London, Prince Consort Road, SW7 2AZ, United Kingdom

Abstract

Topological Insulators (TI) are a recently discovered category of materials. 3D TIs host a protected metallic state on their surface while having an insulating bulk. This state appears in the form of a spin-textured Dirac cone, where spin is locked with momentum (Hasan and Kane 2010). Due to these properties, a wide range of applications are foreseen to exist, from spintronics to superconductors (Pesin and MacDonald 2012). However, more studies and experimental realisation of TI nanomaterials are still lacking.

In this poster, the structural (Pires et al. 2017) and electrical properties of a uniform Sb_2Te_3 thin film fabricated by ion beam sputter deposition are going to be addressed. A discussion on how the thin film bulk conduction is dominated by Variable Range Hopping (VRH) in an Efros and Shklovskii (ES) regime is being showed. However, weak antilocalisation (WAL) cusps on the magnetoresistance at low temperatures and modest magnetic fields are observed, which is indicative of the presence of the TI surface state, having a magnetic localization length L_φ of 62 nm and a single two-dimensional channel open at 2 K. As the thin film has been made using a scalable inexpensive deposition method, the results presented here herald promising future applications of this interesting topological insulator material.

Author Keywords. Topological Insulators, Ion Beam Sputtering Deposition, Variable Range Hopping, Weak Antilocalisation

References

Hasan, M Zahid, and Charles L Kane. 2010. "Colloquium: topological insulators." *Reviews of Modern Physics* 82 (4):3045.

Pesin, Dmytro, and Allan H MacDonald. 2012. "Spintronics and pseudospintronics in graphene and topological insulators." *Nature materials* 11 (5):409.

Pires, A. L., I. F. Cruz, S. Ferreira-Teixeira, P. M. Resende, and A. M. Pereira. 2017. "Bi-Te Thin Film Produced by Ion Beam Sputtering: Impact of Beam Voltage in the Seebeck Coefficient." *Materials Today: Proceedings* 4 (12):12383-12390. doi: https://doi.org/10.1016/j.matpr.2017.10.007.

1D Hematite photoanodes for photoelectrochemical hydrogen production

P. Quitério[1], A. Apolinário[1], C. T. Sousa[1], P. Dias[2], J. Azevedo[1,2], A. M. Mendes[2], J. P. Araújo[1]

[1]IFIMUP-IN, Departamento de Física e Astronomia, Faculdade de Ciências, Universidade do Porto, Portugal
[2]LEPABE, Departamento de Engenharia Química, Faculdade de Engenharia, Universidade do Porto, Portugal

Abstract

Solar-powered technologies for electrochemical production of hydrogen need to be urgently developed. Hydrogen produced via photoelectrochemical (PEC) water splitting cells is pure, sustainable and cost-effective (Gratzel 2001). Research efforts have been devoted to design efficient and stable photoelectrodes using environmentally friendly and cheap materials. Hematite (α-Fe_2O_3) is the most stable metal-oxide semiconductor reported to date (Dias et al. 2016); it is environmentally safe and with a narrow band gap (2.2 eV) displays a theoretical solar-to-hydrogen efficiency as high as 16.8 %. However, the performance of hematite is limited by its poor conductivity and short hole diffusion length, which lead to high electron-hole recombination and poor PEC efficiencies (Sivula, Le Formal, and Grätzel 2011). To overcome such limitations, nanostructuring, in particular 1D nanotubes (NTs) and nanowires (NWs), have emerged as suitable morphologies for an efficient electron transport, preventing recombination losses (LaTempa et al. 2009; Vayssieres et al. 2005). Additional use of dopants, such as Ti or Sn, highly improves the electrical conductivity and PEC performance.

In this work, high aspect-ratio 1D α-Fe_2O_3 nanostructures were prepared, namely NTs by electrochemical anodization of Fe foils (LaTempa et al. 2009) and NWs by hydrothermal method (Vayssieres et al. 2005); at the end, they were annealed using temperatures ranging from 400-800 °C to optimize the crystallinity of hematite. These samples were morphological and structurally characterized by scanning electron microscopy (SEM) and X-ray diffraction (XRD). The PEC performance was evaluated by photocurrent density voltage (*J-V*) curves. The photocurrent showed a favorable increment not only with the use of Ti and Sn dopants, but also with annealing temperature.

Author Keywords. Photoelectrochemical cells, hematite, nanotubes, nanowires.

References

Dias, Paula, António Vilanova, Tânia Lopes, Luísa Andrade, and Adélio Mendes. 2016. "Extremely stable bare hematite photoanode for solar water splitting." *Nano Energy* 23: 70-79. https://doi.org/http://dx.doi.org/10.1016/j.nanoen.2016.03.008..

Gratzel, M. 2001. "Photoelectrochemical cells." *Nature* 414: 338-344.

LaTempa, Thomas J., Xinjian Feng, Maggie Paulose, and Craig A. Grimes. 2009. "Temperature-Dependent Growth of Self-Assembled Hematite (α-Fe2O3) Nanotube Arrays: Rapid Electrochemical Synthesis and Photoelectrochemical Properties." *The Journal of Physical Chemistry C* 113 (36): 16293-16298. https://doi.org/10.1021/jp904560n. https://doi.org/10.1021/jp904560n.

Sivula, Kevin, Florian Le Formal, and Michael Grätzel. 2011. "Solar Water Splitting: Progress Using Hematite (α-Fe2O3) Photoelectrodes." *ChemSusChem* 4 (4): 432-449. https://doi.org/10.1002/cssc.201000416. http://dx.doi.org/10.1002/cssc.201000416.

Vayssieres, L., C. Sathe, S. M Butorin, D. K Shuh, J. Nordgren, and J. Guo. 2005. "One-Dimensional Quantum-Confinement Effect in α-Fe2O3 Ultrafine Nanorod Arrays." *Advanced Materials* 17 (19): 2320-2323. https://doi.org/10.1002/adma.200500992. http://dx.doi.org/10.1002/adma.200500992.

Trapping nanometer sized particles with optical fiber tweezers – a computational study

Sandra M. Rodrigues[1,2], Joana S. Paiva[1,2], Paulo V. S. Marques[1,2], João P. S. Cunha[1,3], Pedro A. S. Jorge[1,2]

[1] INESC TEC, Porto, Portugal

[2] Faculdade de Ciências da Universidade do Porto, Portugal

[3] Faculdade de Engenharia da Universidade do Porto, Portugal

Abstract

Trapping micro-particles using optical fiber-based tools combined with detection and analysis of backscattered radiation can serve as a tool for detection and differentiation of single cells (Ribeiro 2017, Paiva 2018).

In this work we present a computational study of a trapping configuration based on a fiber taper coated with a gold layer of 100 nm and a nanoaperture at its apex. Electric field simulations allowed the calculation of the force acting on the particle at each position, showing a dominance of the gradient force, that enables optical trapping of nanoparticles. By varying the taper's geometry and analyzing how it affected the intensity and electric field gradient maxima of the output field, we defined an optimized geometry. When compared to the simulations of polymeric tips, used in the referenced works, values up to 10 and 15 times larger were found for the intensity and gradient maxima, respectively.

Details towards the experimental realization will be given.

Author Keywords. Optical Trapping, Optical Fiber, Nanoparticles, Gradient Force, Scattering Force

References

Ribeiro, Ana Rita Silva Rodrigues. 2017. "Optical fiber tools for single cell trapping and manipulation". PhD thesis, Faculdade de Ciências da Universidade do Porto.

Paiva, J. S, Ribeiro, R. S. R., Cunha, J. P. S., Rosa, C. C. and Jorge, P. A. S. 2018. "Single Particle Differentiation through 2D Optical Fiber Trapping and Back-Scattered Signal Statistical Analysis: An Exploratory Approach". Em *Sensors 18*. 2018.

On the Development of Organic and Inorganic Thermoelectric Materials for Printing Techniques

João M. Magalhães[1], Ana L. Pires[1], Clara Pereira[2], and André M. Pereira[1]

[1]IFIMUP and IN-Institute of Nanoscience and Nanotechnology, Physics and Astronomy Department, University of Porto, Rua do Campo Alegre s/n, 4169-007 Porto, Portugal.

[2] REQUIMTE/LAQV, Chemistry and Biochemistry Department, Faculty of Sciences, University of Porto, Rua do Campo Alegre s/n, 4169-007 Porto, Portugal.

Abstract

Thermoelectric generators (TEGs) can directly convert waste heat into electrical power (Du, Xu, Paul, and Eklund 2018). Flexible TEGs have been envisaged as an alternative power source for low power consumption devices, such as flexible wearable electronics or devices to be used in remote locations, where the use of bulk materials is precluded by their inherent rigidity. Printing techniques are a possible way to fabricate flexible TEGs by optimizing inks composed by inorganic thermoelectric (TE) materials with high figure of merit (ZT) and combine them with binders, organic solvents, and other additives to produce a printable ink (Pires et al. 2019). However, synthesizing inks for flexible TEGs with high ZT is a challenge due to the poor density and the large concentration of additives which often render a detriment effect on electrical transport (Varghese et al. 2016). In addition, the assembly of TEGs involves contact layers on which the reliability of the device depends. For this reason, solutions to contact issues, including bonding strength, contact resistance, and thermomechanical stress will also need to be addressed (He, Schierning, and Nielsch 2017). Therefore, the main goal of this work is to conceive a flexible and easy printed TEG prototype for energy harvesting using a stencil printing process (see Figure 1). Towards this goal, n-type Bi_2Te_3 TE materials were synthesized by solid-state reaction using a close quart-tube under N_2 atmosphere. Additional, n-type and p-type commercial Bi_2Te_3 TE materials were achieved and used to produce the TEG prototype with a mean particle size up to 50 µm. The inks were formulated with an ionic-conductive polymer, such as PVA, and the three different devices were produced onto polyamide® substrate. All the devices were submitted to thermal treatment and the differences were addressed and discussed.

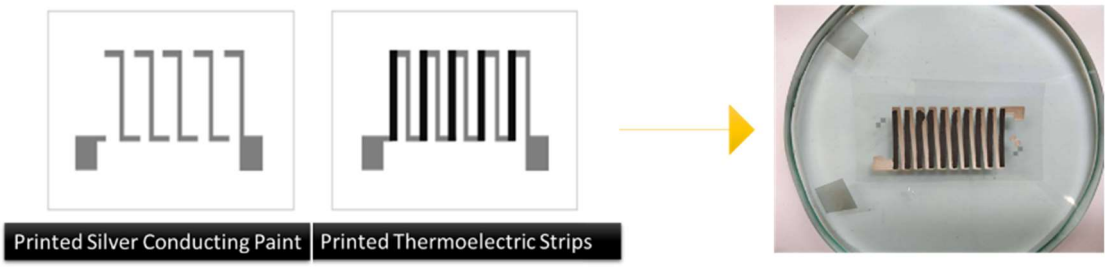

Figure 1: Production of a thermoelectric device using a stencil printing process.

Keywords: Energy harvesting, thermoelectric generator, electronic device, wearable, flexible materials, solid-state reaction, printing techniques, screen printing, stencil printing.

References

Yong Du, Jiayue Xu, Biplab Paul, Per Eklund. 2018. “Flexible thermoelectrics materials and devices”. In *Applied Materials Today*, volume 12.

A. L. Pires, J. A. Silva, M. M. Maia, S. Silva, A. M. L. Lopes, J. Fonseca, M. Ribeiro, C. Pereira, A. M. Pereira. 2019. “Recent advances in functional thermoelectrics materials for printed electronics”. In *Printing Electronics*, Springer.

Tony Varghese, Courtney Hollar, Joseph Richardson, Nicholas Kempf, Chao Han, Pasindu Gamarachchi, David Estrada, Rutvik J. Mehta, Yanliang Zhang. 2016. “High-performance and flexible thermoelectric films by screen printing solution-process nanoplate crystals”. In *Scientific Reports*, article number 6:33135.

Ran He, Gabi Schierning, Kornelius Nielsch. 2017. “Thermoelectric Devices: A Review of Devices, Architectures, and Contact Optimization”. In *Advanced Materials Technologies*, volume 3.

Fiber micro-cantilever displacement detection

Paulo Robalinho and Orlando Frazão

INESC TEC and Department of Physics and Astronomy, Science Faculty of the University of Porto

Abstract

A microsphere combined with a fiber tip is used with a contact sensor functionality. This structure was fabricated with a standard fibre and electric arcs. The tip is centred with the microsphere stem and this occurs during tip formation. Since the study interference results from the interaction of two optical paths whose difference between them results from the tip then the microsphere has no impact on the measurements. This work demonstrates that changing the tip curvature will change these optical paths, which will lead to a change in output power. For the wavelength of 1570 nm, the sensitivity of the geometry to a vibration, for a frequency between 0.2 Hz and 2 Hz is 0.032 ± 0.001 (Hz^{-1}) and the temperature sensitivity for the range of 22 °C and 55 °C is non-linear.

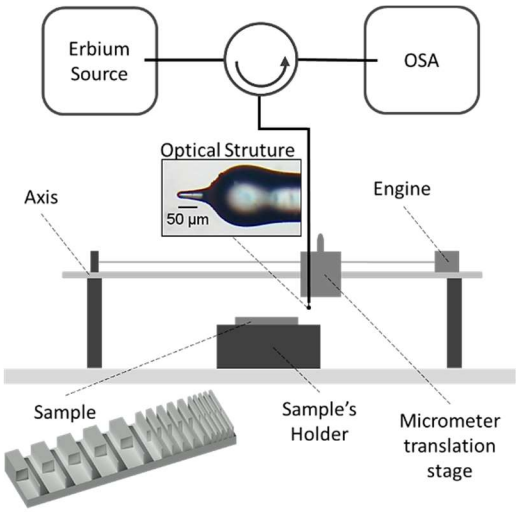

Figure 12: Assembly scheme and sensor.

Author Keywords. Physic, Optic, Fibre, Sensor, Contact Sensor, Cantilever, Detection, Vibration

References

Andres H. La Rosa and Hans D. Hallen. 2002. "Compact method for optical induction of proximal probe heating and elongation". In Optical Society of America, 41(10), 2015-2019.

Limin Zou, He Ni, Peng Zhang and Xuemei Ding. 2017. "Assembled Cantilever Fiber Touch Trigger Probe for Three-Dimensional Measurement of Microstructures". In Sensor, 17, 2652.

S. Hoen, H. J. Mamin and D. Rugar. 1993. "Thermomechanical data storage using a fiber optic stylus". In Applied Physics Letters 64, 267-269.

Transmission Properties of Optical Fibers during Taper Fabrication: Adiabaticity, Mode Dissipation, and Diameter Control

Filipe Marques, Orlando Frazão

INESC-TEC, Faculdade de Ciências, Universidade do Porto, Rua do Campo Alegre, s/n, 4169-007 Porto, Portugal.

Abstract

The transmission properties of standard telecommunication optical fibers (Corning® SM-28®) are monitored during taper pulling. The tapers are fabricated by *heat-and-pull* using a microheater (MHI Fibheat 200) and two motorized pulling stages (OWIS PS10). Micron-sized waist-diameter adiabatic tapers with low loss at 1550-nm are fabricated. We present a simple technique for real-time diameter control based on the intensity drops due to mode dissipation, on the transmission profile of an 800-nm wavelength laser diode. This enables accurate mode selection and filtering.

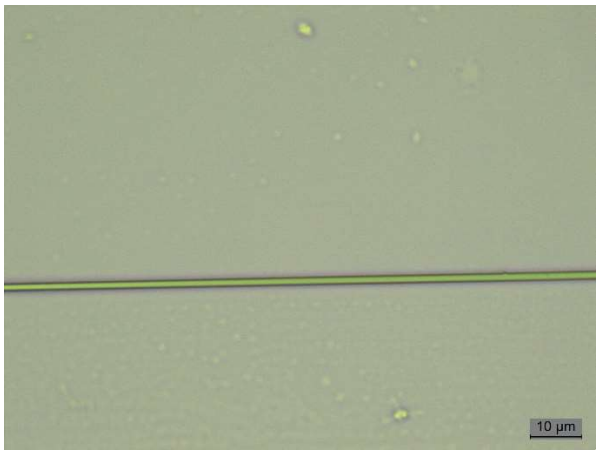

Figure 13. Optical Microscope image of a tapered fiber with a waist diameter of about 2.0 µm.

Author Keywords. Optical Fiber Tapers, Adiabatic Tapers, Mode Dissipation, Diameter Monitoring.

References

1. T. A. Birks and Y. W. Li. 1992. “The Shape of Fiber Tapers”. In *Journal of Lightwave Technology*. 432-438
2. L. Tong, J. Lo, and E. Mazur. 2004. “Single-mode guiding properties of subwavelength diameter silica and silicon wire waveguides” in *Optics Express*. 1025-1035. OSA Publishing
3. M. C. Frawley, A. Petcu-Colan, V. G. Truong and S. N. Chormaic. 2012. “Higher order mode propagation in an optical nanofiber”. In *Optics Communications*. 285(23). 4648-4654.

Exploring cosmological systems under alternative theories of gravity using the Schrödinger-Poisson formalism

Tiago D. Ferreira[1,2], Nuno A. Silva[1,2], O. Bertolami[1,3], C. Gomes[1,3] and Ariel Guerreiro[1,2]

[1] Department of Physics and Astronomy, Faculty of Sciences, University of Porto, R. Campo Alegre, 4169-007, Porto, Portugal

[2] INESC TEC - CAP, R. Campo Alegre, 4169-007, Porto, Portugal

[3] Centro de Física do Porto, R. Campo Alegre, 4169-007, Porto, Portugal

Abstract

The Theory of General Relativity provides a successful description for gravity, however, at cosmological scales, this success is only achieved through the introduction of dark-matter and dark-energy. Moreover, the incompatibility with Quantum Mechanics suggests that General Relativity is not the final description of gravity. In order to overcome these problems, extensions of General Relativity have been proposed. Studying the implications of these new extensions is crucial to understand their validity and agreement with the available observational data. However, these models tend to be fairly complex, making their analytical treatment very difficult or even impossible. Fortunately, in the weak field limit, the original problem is reduced to a Generalized Schrödinger-Poisson system, a mathematical model that describes a wide class of physical models, including light propagating in nonlocal media. Therefore, the numerical solvers developed for these last systems can be adapted to simulate the former. In this work, we discuss the adaptations made to the solvers, originally developed for simulating light in nonlocal systems, to tackle the dynamics of large distributions of matter whose interaction is governed by extensions of the Theory of General Relativity, namely those based on non-minimal coupling between curvature and matter. In particular, the structure of the resulting simulation module, its performance, and its testing are analyzed.

Author Keywords. Schrödinger-Poisson equation, local and nonlocal nonlinear optical systems, Theory of General Relativity, non-minimal coupling models, GPGPU supercomputing, HiLight simulation platform

References

[1] - R. Johnston, A. N. Lasenby, and M. P. Hobson, Cosmological fluid dynamics in the Schrödinger formalism, Monthly Notices of the Royal Astronomical Society 402, 2491–2502 (2010).

[2] - O. Bertolami, C. G. Bohmer, T. Harko, and F. S. N. Lobo, ¨ Extra force in f(R) modified theories of gravity, Physical Review D 75, 104016 (2007).

[3] - O. Bertolami, C. Gomes, and F. S. N. Lobo, Gravitational waves in theories with a nonminimal curvature-matter coupling, The European Physical Journal C 78, 303 (2018).

A multidimensional solver of the generalized Schrödinger equation based on GPGPU supercomputing

Tiago D. Ferreira[1,2], Nuno A. Silva[1,2] and Ariel Guerreiro[1,2]

[1] Department of Physics and Astronomy, Faculty of Sciences, University of Porto, R. Campo Alegre, 4169-007, Porto, Portugal

[2] INESC TEC - CAP, R. Campo Alegre, 4169-007, Porto, Portugal

Abstract

The Generalized Schrödinger equation with both local and nonlocal nonlinearities has been used to model a wide variety of phenomena in multiple fields of Physics. For example, in optics, it can describe the propagation of light in either a Kerr medium or in a nematic liquid crystal. It also appears in the context of gravitation and cosmology to describe the gravitational interaction between matter. This versatility of this model has led it to constitute the basis to develop optical analogues and perform optical simulations. Therefore, being able to obtain solutions to these equations in systems with high dimensionality is of paramount importance, which usually is too difficult to obtain using purely analytical methods. As a result, numerical tools must be employed not only to gain better insight on the phenomena being under analysis but also, and perhaps more importantly, as a support in the development of real experimental setups that can test our understandings.

In this work, we report the development of a high-performance multidimensional solver with parallel techniques based on GPGPU supercomputing capable of addressing these different scenarios, with the possibility of coupling the different fields through the different nonlinearities. The numerical methods, the structure of the simulation model and its tests and performance are analyzed.

Author Keywords. Generalized Schrödinger equation, Schrödinger-Newton equation, Optical analogues, Local and nonlocal nonlinear optical systems, GPGPU supercomputing, HiLight simulation platform

References

T. D. Ferreira, N. A. Silva, and A. Guerreiro, Superfluidity of light in nematic liquid crystals, Physical Review A 98, 023825 (2018).

N. A. Silva, J. T. Mendonça, and A. Guerreiro, Persistent currents of superfluidic light in a four-level coherent atomic medium, J. Opt. Soc. Am. B 34, 2220 (2017).

T. Roger, C. Maitland, K. Wilson, N. Westerberg, D. Vocke, E. M. Wright, and D. Faccio, Optical analogues of the Newton–Schrödinger equation and boson star evolution, Nature Communications 7 (2016), 10.1038/ncomms13492.

D. Vocke, T. Roger, F. Marino, E. M. Wright, I. Carusotto, M. Clerici, and D. Faccio, Experimental characterization of nonlocal photon fluids, Optica 2, 484 (2015)

Low Noise Power Supply Board

R. Fernandez[2], G. Evans [2,4], J. Augusto[2,3],L. Gurriana[1], A. Gomes [1,2]

[1] Laboratório de Instrumentação e Física Experimental de Partículas, LIP

[2] Faculdade de Ciências da Universidade de Lisboa, FCUL

[3] Instituto de Engenharia de Sistemas e Computadores, Investigação e Desenvolvimento em Lisboa, INESC-ID

[4] Instituto de Biofísica e Engenharia Biomédica, IBEB

Abstract

The current system that distributes high voltage to the hadronic calorimeter TILECAL of the ATLAS experiment at CERN was manufactured in the late 1990s and now many of its components are obsolete. In addition to this, the continuous exposition to high levels of radiation that results from the LHC collision affects the whole system. Given this, an update was proposed to surpass these problems: a new board would implement a remote system that would minimize the amount of radiation received and maximize the reliability and robustness of the system. For this new system it is necessary to produce a board that provides the necessary supplies for the new remote voltage distribution system. Therefore, the presented work consists in the development of a power supply board capable of providing both high voltage, -830 V and -950 V, and low voltage, ±12 V and 3.3 V, with low noise, resorting to DC/DC converters. The high voltage is digitally controlled so each photomultiplier of the detector can receive the right voltage to work correctly. Besides that, this board is controlled by SPI protocol and has an ADC that is used to provide the user monitoring of the voltages and currents in real-time.

Author Keywords. CERN, ATLAS, Power Supply, Low Noise

References

C. O'Luanaigh, “The Large Hadron Collider,” CERN, 21 Janeiro 2014. [Online]. Available: https://home.cern/topics/large-hadron-collider.

P. Vankov, “ATLAS Upgrade for the HL-LHC: meeting the challenges of a five-fold increase in collision rate,” em *EPJ Web of Conferences - Hadron Collider Physics symposium*, 2011.

F. Vazeille, “Performance of a Remote High Voltage Power Supply for the Phase II Upgrade of the ATLAS Tile Calorimeter,” CERN, Genebra, 2015.

D. Kalinsky e R. Kalinsky, “Introduction to Serial Peripheral Interface,” Embedded , 1 Fevereiro 2002. [Online]. Available: http://www.embedded.com/electronics-blogs/beginner-s-corner/4023908/Introduction-to-Serial-Peripheral-Interface.

IEEE Standard for terminology and test methods for analog-to-digital converters. IEEE Std. 1241-2010 (Revision of IEEE Std. 1241-2000), 2010.

Functional Tester for High Voltage Boards of the TileCal Calorimeter

Filipe Cuim[2], J. Augusto[2,3], G. Evans[2,4], A. Gomes[1,2], F. Martins[1]

[1] LIP Laboratório de Instrumentação e Física Experimental de Partículas

[2] FCUL Faculdade de Ciências da Universidade de Lisboa

[3] INESC ID Instituto de Engenharia de Sistemas e Computadores, Investigação e Desenvolvimento em Lisboa

[4] IBEB Instituto de Biofísica e Engenharia Biomédica

Abstract

TileCal, the Hadronic Calorimeter of the ATLAS experiment at CERN, is being upgraded in order to fit the requirements of the High-Luminosity LHC. The high-voltage (HV) distribution card (that supplies and regulates the voltage of the photomultipliers) is one of the systems that is being upgraded. The current one is located on the detector, which means that particles originated from the collisions will damage the associated electronic components of the HV card. One proposed solution consists on putting the HV board in the ATLAS cavern (away from the detector) and distributing the High Voltage using long multi-conductor cables. This work is about the development of a functional tester and a graphical interface for controlling the HV boards that will be supplying the photomultipliers of the detector. A Raspberry Pi will be used to link the HV boards to a PC user interface, allowing the control and test of the entire system. This interface is being designed in Python, where each HV Board will have its own class, therefore simplifying the hierarchy of communications. The Raspberry Pi and the HV board will communicate via the protocol SPI (Serial Peripheral Interface) and the communication with the PC is done via Ethernet.

Author Keywords. Raspberry Pi, SPI, Python, TileCal, ATLAS.

References

C. O'Luanaigh, "The Large Hadron Collider," CERN, 21 Janeiro 2014. [Online]. Available: https://home.cern/topics/large-hadron-collider.

P. Vankov, "ATLAS Upgrade for the HL-LHC: meeting the challenges of a five-fold increase in collision rate," em *EPJ Web of Conferences - Hadron Collider Physics symposium*, 2011.

F. Vazeille, "Performance of a Remote High Voltage Power Supply for the Phase II Upgrade of the ATLAS Tile Calorimeter," CERN, Genebra, 2015.

D. Kalinsky e R. Kalinsky, "Introduction to Serial Peripheral Interface," Embedded , 1 Fevereiro 2002. [Online]. Available: http://www.embedded.com/electronics-blogs/beginner-s-corner/4023908/Introduction-to-Serial-Peripheral-Interface.

New Optochemical sensor for dissolved CO_2 evaluation: results from application to a recirculation aquaculture system and bacterial microcosms

J.P. Mendes[1,2,4], L. Coelho[2], C. Pereira[1], B. Kovacs[3], P. Jorge[2] and M.T. Borges[4,5]

[1] CIQUP & Chemical and Biochemical Department, Faculty of Sciences, Porto University, Portugal

[2] INESCTEC – Institute for Systems and Computer Engineering, Technology and Science, Portugal

[3] Department of General and Physical Chemistry, Pécs University, Pécs, Hungary

[4] CIIMAR - Interdisciplinary Centre of Marine and Environmental Research, Porto University, Portugal

[5] Department of Biology, Faculty of Sciences, Porto University, Portugal

Abstract

Dissolved carbon dioxide (dCO2) evaluation is very important in different fields. There are some different methods for CO2 measurements, including potentiometry, UV/Vis spectrophotometry and IR spectrometry (Mills and Yusufu 2016). These methods are time-consuming and inappropriate for real-time monitoring. Recently, several authors developed optical fiber-based technology for dCO2 detection (Thomas et al. 2017; Davenport et al. 2017). In this work, it was developed a new, integrated, colorimetric-optical fiber-based system for dCO2 monitoring in aquaculture industry. The sensing chemistry is based on colorimetric changes of the used polymeric indicator – *poly p-nitrophenol* – in contact with CO2. The sensing membrane was attached to an optical fiber probe (transmission mode) and Illuminated with an integrated dual wavelength LED. Validation tests were done in situations simulating real environments, focusing in different fields of application. The results have shown the suitability of the new sensor for assessing dCO2 dynamics and its fast detection in different conditions.

Author Keywords. colorimetric sensor, optical fiber, dissolved carbon dioxide, *aquaculture*.

References

Davenport, J. J., M. Hickey, J. P. Phillips, and P. A. Kyriacou. 2017. "Dual pO2/pCO2 fibre optic sensing film." *Analyst* 142 (10): 1711-1719. https://doi.org/10.1039/c7an00173h. https://www.ncbi.nlm.nih.gov/pubmed/28401218.

Mills, Andrew , and Dilidaer Yusufu. 2016. "Extruded colour-based plastic film for the measurement of dissolved CO 2." *Sensors and Actuators B: Chemical* 237: 1076-1084. https://doi.org/10.1016/j.snb.2016.07.141.

Thomas, Peter J., Dariia Atamanchuk, Jostein Hovdenes, and Anders Tengberg. 2017. "The use of novel optode sensor technologies for monitoring dissolved carbon dioxide and ammonia concentrations under live haul conditions." *Aquacultural Engineering* 77: 89-96. https://doi.org/10.1016/j.aquaeng.2017.02.004.

Detection of hydrogen peroxide using a chemiluminescence technique: preliminary study

Helena Vasconcelos[1,2], José M. M. M. de Almeida[2,4], Cristina Saraiva[1], P.A.S. Jorge[2,3] and L. Coelho[2]

[1]School of Agrarian and Veterinary Sciences, CECAV-Centro de Ciência Animal e Veterinária, Univ. of Trás-os-Montes e Alto Douro, 5001-801 Vila Real, Portugal; hcgv@inesctec.pt, crisarai@utad.pt

[2]INESC TEC - Technology and Science and Faculty of Sciences, Univ. of Porto, Rua do Campo Alegre, 4169-007 Porto, Portugal; lcoelho@inesctec.pt

[3]Dep. of Physics and Astronomy of Faculty of Sciences, Univ. of Porto, 4169-007 Porto, Portugal; pedro.jorge@fc.up.pt

[4]Dep. of Physics, School of Science and Technology, Univ. of Trás-os-Montes e Alto Douro, 5001-801 Vila Real, Portugal; jmmma@utad.pt

Abstract

Nowadays, food safety has as its main objective to provide safe food to consumers.

BA (biogenic amines) are used as an indication of food spoilage (Sørensen et al. 2018), the determination of their concentration in foods is an important method of food control (Erim 2013). BA are nitrogenous organic bases of low molecular weight (Cunha, Lopes, and Fernandes 2017).

BA do not have chemiluminescence properties, but hydrogen peroxide (H_2O_2), which is a side product of its degradation by the enzyme such as, diamine oxidase, is used to obtain luminescence when reaction with 5-amino-2,3-dihydrophthalazine-1,4-dione ($C_8H_7N_3O_2$) occurs (Omanovic-Miklicanin and Valzacchi 2017).

In this work, we present a chemiluminescence based technique to measure small quantities of H_2O_2 added to a membrane consisting of hydroxyethyl cellulose. The results of this study shown that with this method it is possible to detect very low concentrations of H_2O_2 down to 0.01%w/w.

Author Keywords. Biogenic amines, Chemiluminescence, Food storage.

References

Cunha, S C, R Lopes, and J O Fernandes. 2017. "Biogenic Amines in Liqueurs: Influence of Processing and Composition." *Journal of Food Composition and Analysis* 56: 147–55. https://doi.org/10.1016/j.jfca.2016.11.016.

Erim, F Bedia. 2013. "Recent Analytical Approaches to the Analysis of Biogenic Amines in Food Samples." *TrAC - Trends in Analytical Chemistry*. Elsevier Ltd. https://doi.org/10.1016/j.trac.2013.05.018.

Omanovic-Miklicanin, Enisa, and Sandro Valzacchi. 2017. "Development of New Chemiluminescence Biosensors for Determination of Biogenic Amines in Meat." *Food Chemistry* 235 (14412007): 98–103. https://doi.org/10.1016/j.foodchem.2017.05.031.

Sørensen, Klavs Martin, Violetta Aru, Bekzod Khakimov, Ulrik Aunskjær, and Søren Balling Engelsen. 2018. "Biogenic Amines: A Key Freshness Parameter of Animal Protein Products in the Coming Circular Economy." *Current Opinion in Food Science* 22: 167–73. https://doi.org/10.1016/j.cofs.2018.05.014.

Effect of radiation on the electrolyte of a solid-state battery

José Brandão[1], Joana Oliveira[2], Maria H. Braga[2]

[1]Department of Physics and Astronomy, Sciences Faculty, Porto University, Rua do Campo Alegre, 4169-007 Porto, Portugal

[2] Physics Engineering Department, Engineering Faculty, Porto University, Rua Dr. Roberto Frias, 4200-465 Porto, Portugal

Abstract

Solid-state batteries are a new safe and inexpensive format of energy storage, in contrast with the lithium-ion batteries which are flammable due to the liquid electrolyte. The solid electrolyte is a glassy-amorphous material ($A_{2.99}Ba_{0.005}ClO$, with A=Li or Na). Conditioning of the glass involves the optimization of A_2O and AO^- electric dipoles interaction to form long ferroelectric molecules aligned by the internal electric field (Braga 2017); a great alignment increases the cell capacity and can be improved trough temperature treatment and aging process.

This dielectric material presents unusual properties (Braga 2018) as a huge dielectric constant ($\varepsilon > 10^6$ at 25°C), granting a high cell capacity and high ion conductivity ($\sigma_i > 10^{-2} Scm^{-1}$ at 25 °C) making it a perfect candidate for these new types of batteries. Moreover, the electrolyte is a ferroelectric material and, as such, piezo- and pyroelectric.

One process of improving the ferroelectric performance might be through radiation exposure. The exposition the electrolyte to different types of high-power radiation (from infrared to ultraviolet) is being explored; the impact of radiation in the internal resistance of the electrolyte, on the cell open circuit voltage (OCV) and on the cell capacity.

Author Keywords. Solid-state, batteries, electrolyte, ferroelectric, radiation.

References

M. H. Braga, J. A. Ferreira, A. J. Murchison, J. B. Goodenhough, "Electric Dipoles and Ionic Conductivity in a Na^+ Glass Electrolyte", *J. Electrochem. Soc. 2017 volume 164, issue 2, A207-A213.* DOI: 10.1149/2.0691702jes.

M. H. Braga, J. E. Oliveira, T. Kai, A. J. Murchison, A. J. Bard, J. B. Goodnough, "Extraordinary dielectric properties at heterojunction of amorphous ferroelectrics", *J. Am. Chem. Soc.*, 2018, 140 (51), pp 17968–17976. DOI: 10.1021/jacs.8b09603.

M. H. Braga, N. S. Grundish, A. J. Murchison and J. B. Goodenough, "Alternative strategy for a safe rechargeable battery", *Energy Environ. Sci., 2017, 10, 331.* DOI: 10.1039/c6ee02888h

Acknowledgments

The COMPETE2020 and FCT project, EU and Portugal,PTDC/CTM-ENE/2391/2014

Micropatterning Organic Single Crystals for Photonic Sensor Applications

J. M. Serra[1], S. I. Sequeira[1,2], I. Domingos[3], A. P. Oliveira[3], E. Maçôas[2], S. Cardoso[1,2], H. Alves[2,3], D. C. Leitão[1,2]

[1] INESC Microsystems and Nanotechnologies, rua Alves Redol 9, 1000-029 Lisbon, Portugal

[2] Instituto Superior Técnico, Universidade de Lisboa, Av. Rovisco Pais 1, 1049-001 Lisbon, Portugal

[3] UA-CICECO, University of Aveiro, Campus Universitário de Santiago, 3810-193 Aveiro, Portugal

Abstract

Organic single crystals (OSCs) have huge potential for new integrated photonic devices due to attractive light absorption properties in the visible range (Fang 2014). OSCs provide an alternative material for photosensors with applications in visible light communication (Figueiredo 2017), for example. OSCs present exciton conduction, where the electric current is a result of excitons (excited electron-hole pairs in the crystal) diffusing through the lattice. This is the origin of photoconductivity in OSCs: a photon will excite a charge carrier, generating an exciton, which can be collected to obtain an electric current. Additional mechanisms which enhance device efficiency can take place. Rubrene, an OSC widely used in organic electronics, presents a charge mobility of 40 cm^2/V s, much higher than that of amorphous Si (under 1 cm^2/V s) (Takeya 2007), making it a very suitable material for photosensor applications. Still, large-scale fabrication of fully integrated photonic devices demands new strategies to include OSCs in a semiconductor fabrication line. Most conventional fabrication techniques typically used in integrated circuit production can be incompatible with organic crystals, leading to physical damage, which may affect the final device performance (Li 2010). In this work we delivered an innovative fabrication protocol to allow the use of standard cleanroom techniques (optical lithography and Reactive Ion Etching (RIE)) for OSC micro-patterning onto Si substrates for device integration.

In previous works, rubrene single crystals grown by physical vapor transport were directly laminated on glass and subsequently connected to macroscopic contacts with carbon ink (Pinto 2014). To enable chip integration of the devices, we begin the process by laminating the rubrene OSCs over pre-patterned Au contacts (Fig. 1a). A protection layer is then spin-coated on top of the laminated crystals. This is followed by optical lithography to define the device size and geometry. To transfer the pattern to the crystal, RIE conditions were optimized for different gas combinations, with an etch rate of 1.63 ± 0.87 Å/s. The etching process end point control is performed visually. As rubrene crystals fluoresce when optically excited under a 468 nm wavelength, confocal fluorescence microscopy was also used to verify the complete etch of the organic single crystals. The patterned devices are then characterized for their opto-electronic behavior.

In Fig 1b. we show a fluorescence image of a patterned crystal obtained with confocal microscopy, with Fig 1c. showing the fluorescence spectrum in the regions delimited in Fig 1b. These images show that full patterning of the rubrene single crystals was successfully achieved by this protocol, proving it as a viable step towards fully integrated OSC microfabricated devices. Most recent results on photocurrent measurements and the impact of the microfabrication process on the device performance will be discussed further.

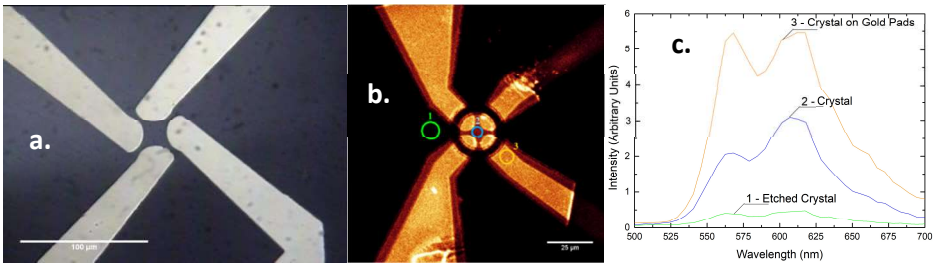

Figure 1. (a) Laminated crystal on top of microfabricated Au contacts, before crystal patterning. (b) Confocal fluorescence microscope image of patterned organic single crystal. (c) Fluorescence spectra acquired in the regions defined in Fig. 1b.

Author Keywords. Organic single crystals, reactive ion etching, microfabrication.

References

Fang, Hong-Hua, Ran Ding, Shi-Yang Lu, Yue-De Yang, Qi-Dai Chen, Jing Feng, Yong-Zhen Huang, and Hong-Bo Sun. "Whispering-gallery mode lasing from patterned molecular single-crystalline microcavity array." *Laser & Photonics Reviews* 7, no. 2 (2013): 281-288.

Figueiredo, Monica, Luis Nero Alves, and Carlos Ribeiro. "Lighting the wireless world: The promise and challenges of visible light communication." *IEEE Consumer Electronics Magazine* 6, no. 4 (2017): 28-37.

Takeya, J., M Yamagishi, Y. Tominari, R. Hirahara, Y. Nakazawa, T. Nishikawa, T. Kawase, T. Shimoda, and S. Ogawa. "Very high-mobility organic single-crystal transistors with in-crystal conduction channels." *Applied Physics Letters* 90, no. 10 (2007): 102120.

Li, Rongjin, Wenping Hu, Yunqi Liu, and Daoben Zhu. "Micro-and nanocrystals of organic semiconductors." *Accounts of chemical research* 43, no. 4 (2010): 529-540.

Pinto, Rui M., Ermelinda MS Maçôas, and Helena Alves. "Enhanced conductivity and photoresponse at a rubrene single-crystal–PCBM film interface." *Journal of Materials Chemistry C* 2, no. 18 (2014): 3639-3644.

AUTHORS INDEX

ISBN: 978-972-752-250-7

www.fe.up.pt/dce19
dce@fe.up.pt